What do We Learn From X-ray Observations of Supernovae and Supernova Remnants?

Dan Patnaude (SAO)

C. Badenes (Pitt); D. Castro (SAO); D. Ellison (NCSU); R. Fesen (Dartmouth); T. Jacovich (GWU/SAO); J. Laming (NRL); S.H. Lee (Kyoto); R. Margutti (Northwestern); D. Milisavljevic (Purdue); S. Nagataki (RIKEN); P. Slane (SAO); J. Vink (UvA); K. Weil (Dartmouth)

G292.0+1.8

W49B

Kepler's SNR

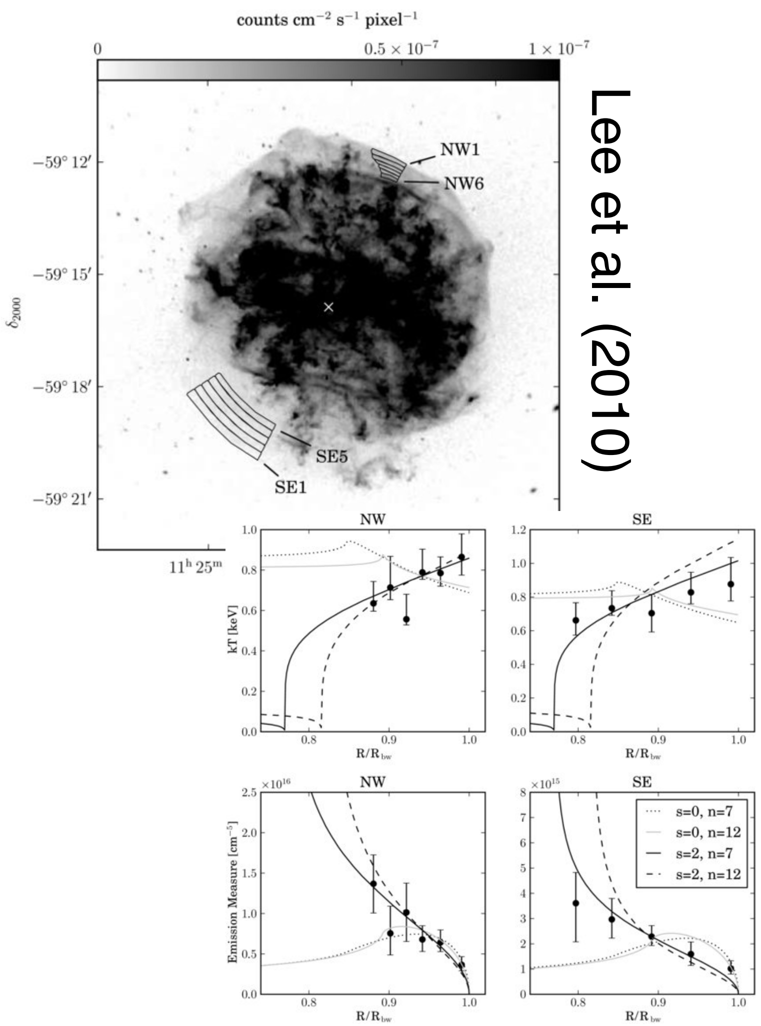

Lee et al. (2010)

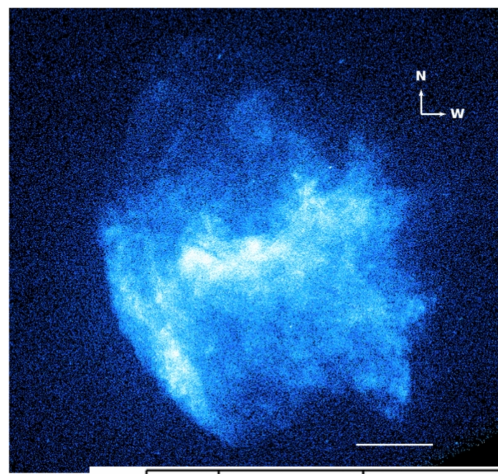

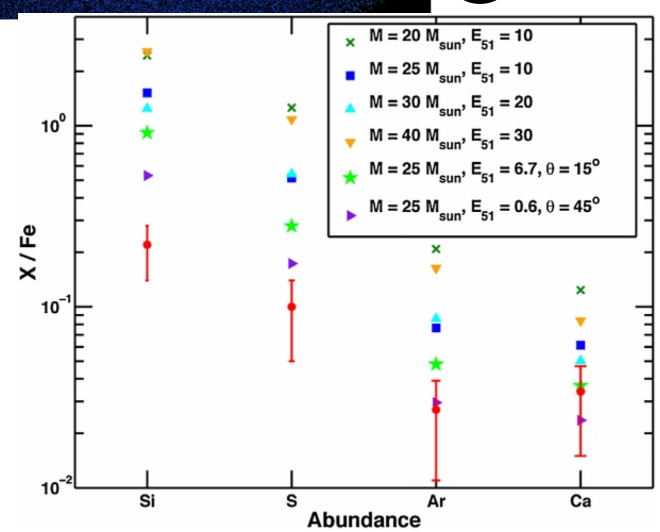

Lopez et al. (2013)

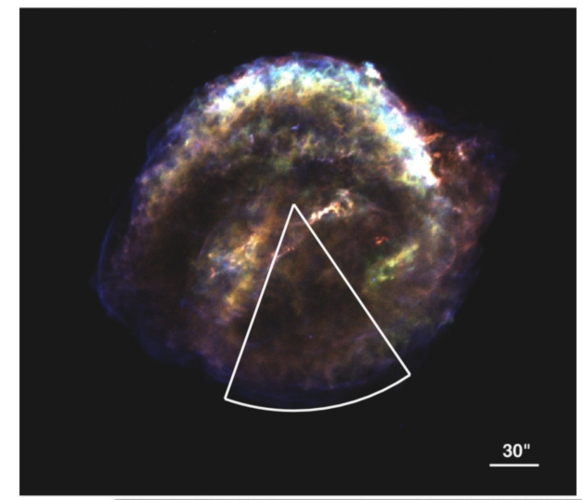

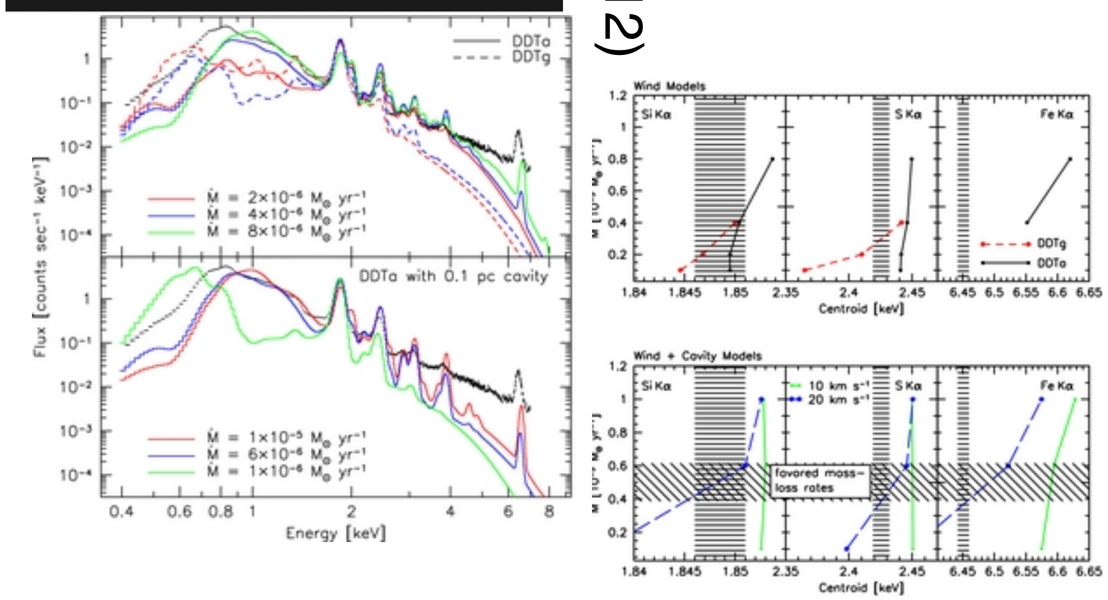

Patnaude et al. (2012)

- Progenitor Evolution
- SN Energetics and Compact Objects
- Ia Progenitors and SNe

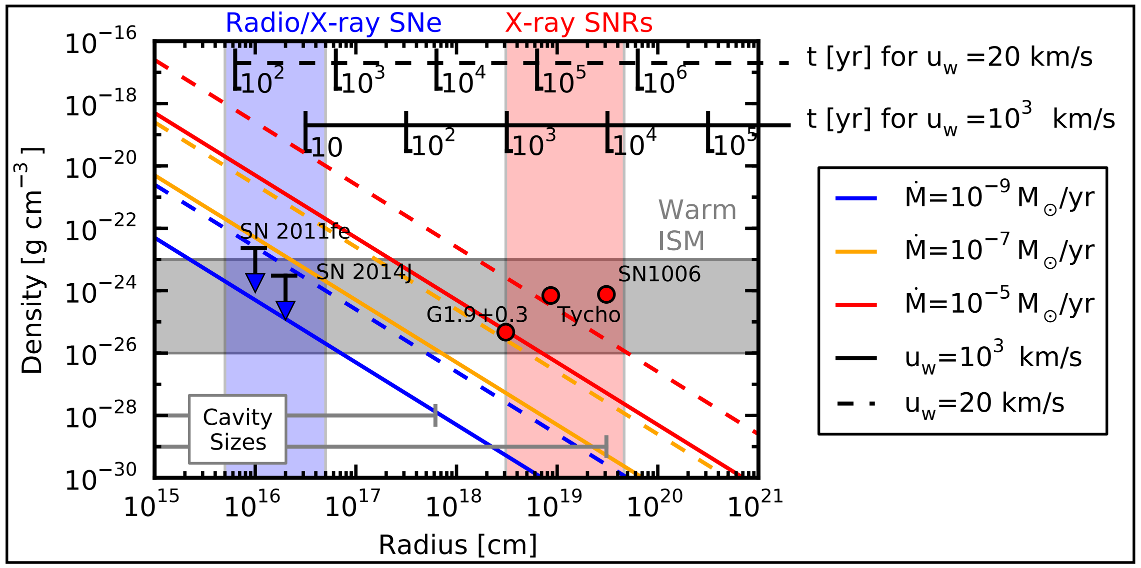

Patnaude and Badenes (2017)

SNR probe a much earlier phase of evolution in their progenitor systems

X-ray properties and SNR dynamics directly reflect the progenitor's evolution, its environment, and the machinations of the explosion (see posters S2.8 (Jacovich), S10.8 (Katsuragawa), S10.12 (Matsuoka), and S10.19 (Yasuda))

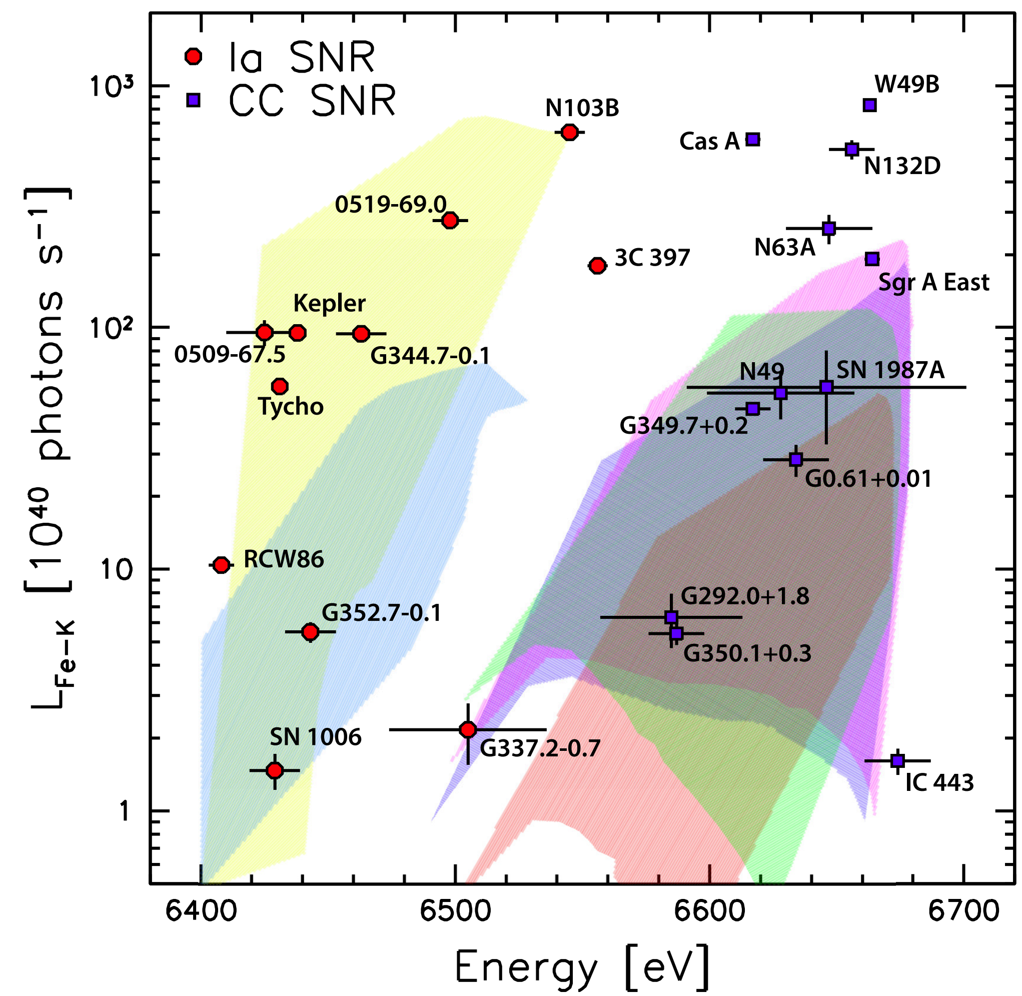

Patnaude et al. (2015)

A Monitoring Program of Cas A

Only nearby SNR to show yearly variations in thermal and nonthermal emission, and also evidence for a young and evolving neutron star

- thermal emission traces structure of ejecta and circumstellar environment
- nonthermal emission informs us on magnetic field amplification and diffusive shock acceleration
- changes in neutron star emission test models for solid state astrophysics

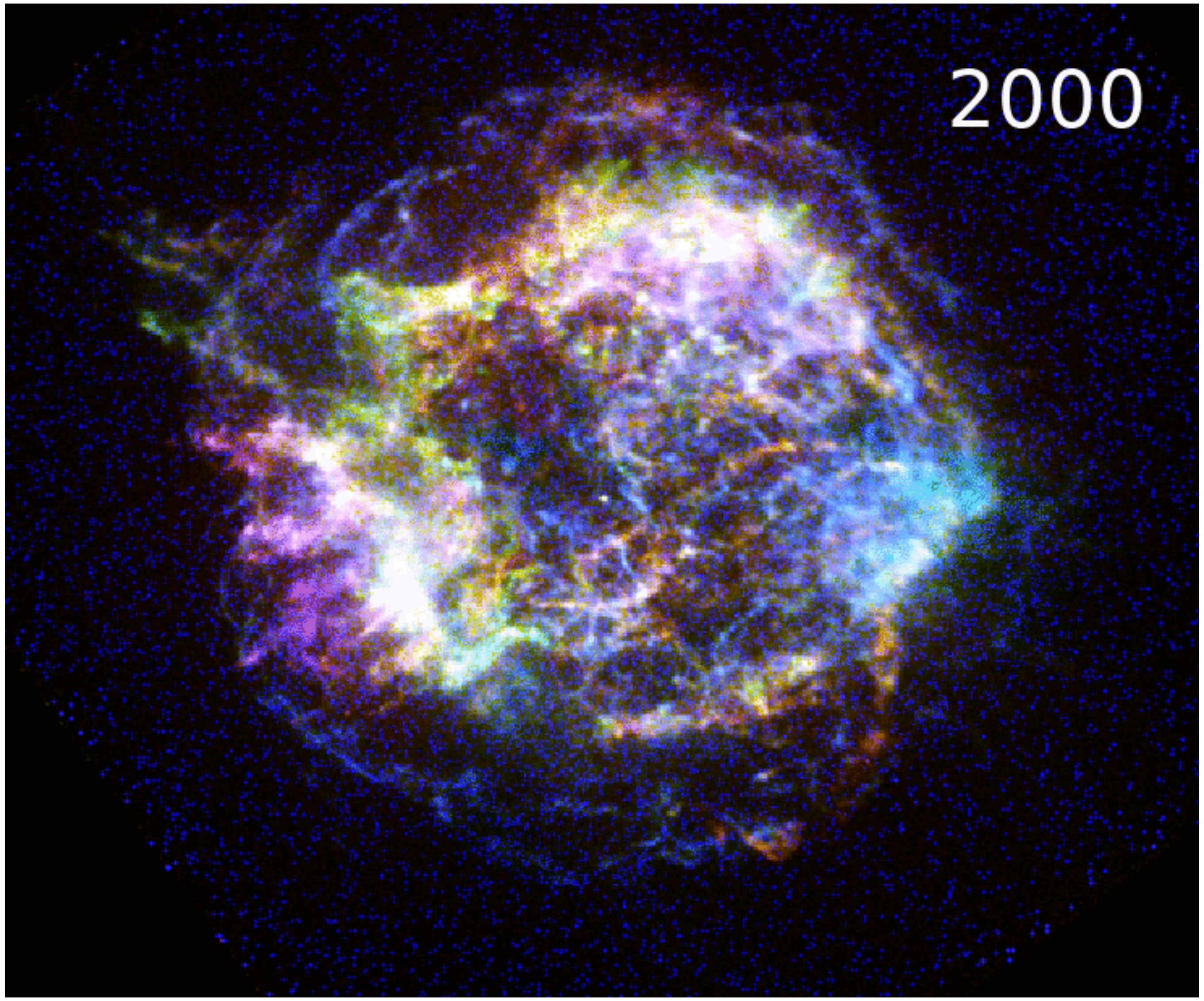

A Monitoring Program of Cas A

Only nearby SNR to show yearly variations in thermal and nonthermal emission, and also evidence for a young and evolving neutron star

- thermal emission traces structure of ejecta and circumstellar environment
- nonthermal emission informs us on magnetic field amplification and diffusive shock acceleration
- changes in neutron star emission test models for solid state astrophysics

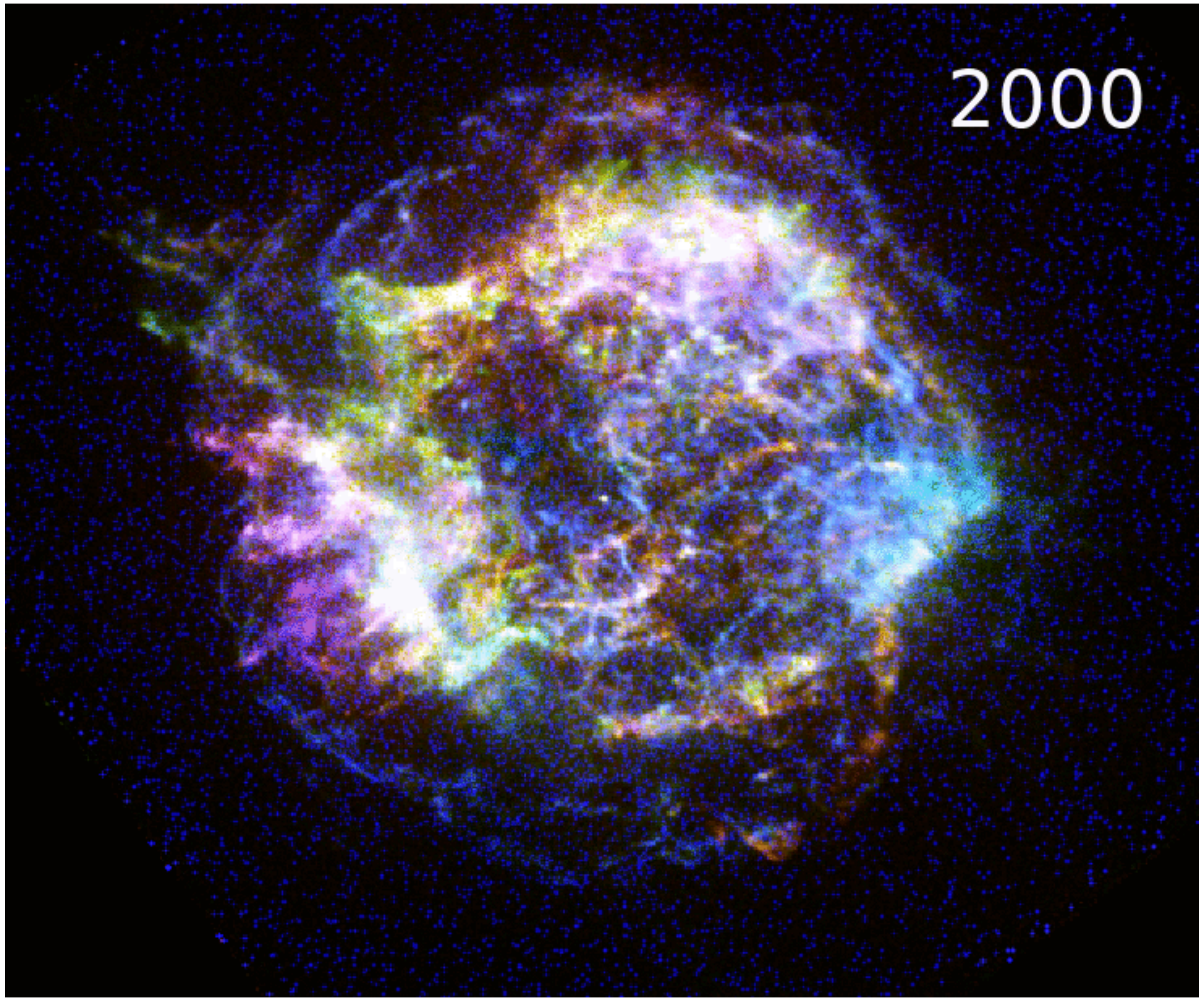

For each epoch from 2000 - 2018:

- pixels are selected using a Weighted Voroni Tesselation with S/N > 80 (> 1000 counts/region)
- due to the bulk expansion of Cas A, the region locations and number of regions are epoch dependent
- spectral parameters in any region are a convolution of the emission from that region and contributions from adjacent pixels
- use WVT mask to inform fitting parameters

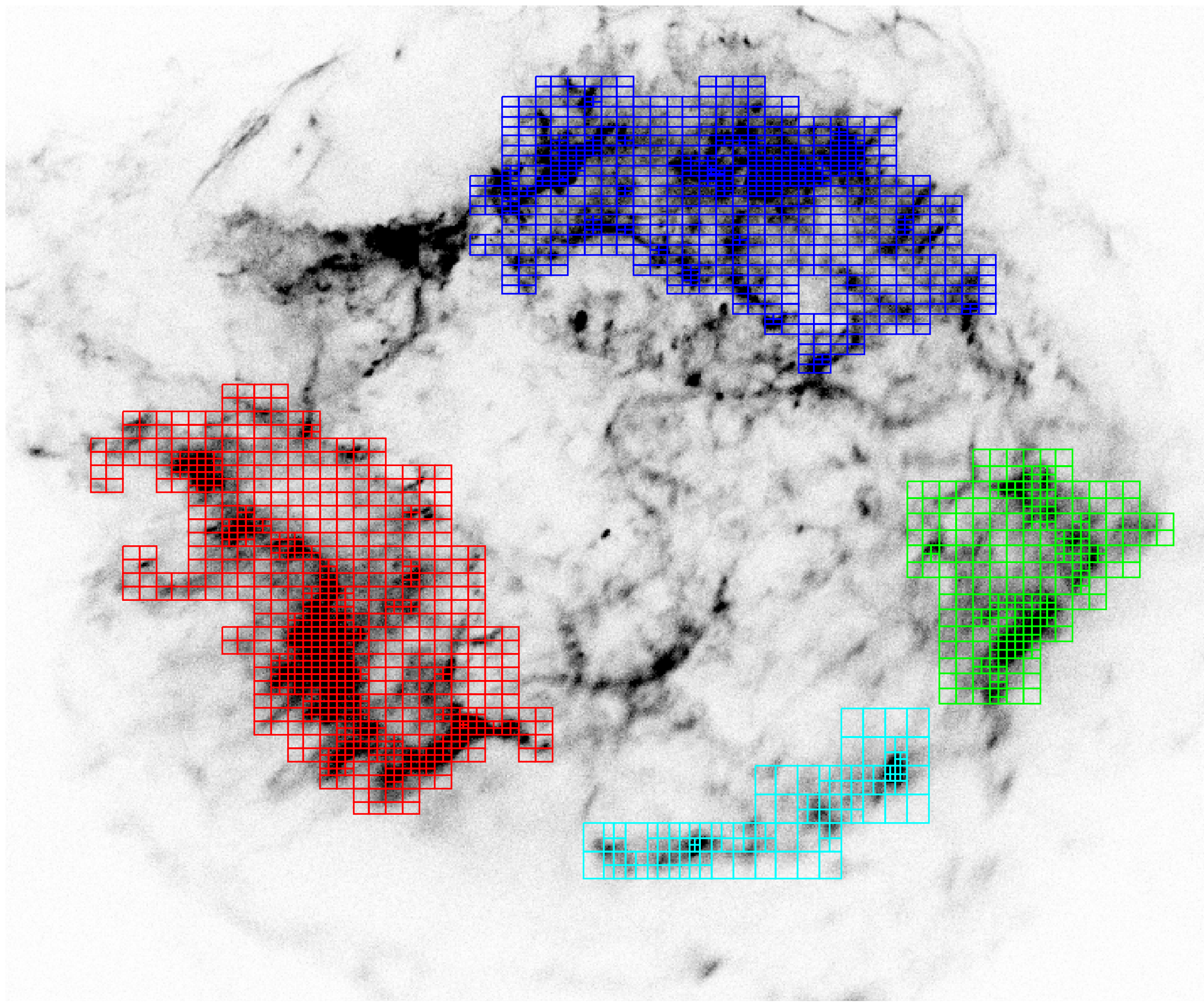

Broadband X-ray image of Cas A with WVT selected regions overlaid

For each epoch from 2000 - 2018:

- pixels are selected using a Weighted Voroni Tesselation with S/N > 80 (> 1000 counts/region)
- due to the bulk expansion of Cas A, the region locations and number of regions are epoch dependent
- spectral parameters in any region are a convolution of the emission from that region and contributions from adjacent pixels
- use WVT mask to inform fitting parameters

$$p_i = \frac{\sum_{i \neq j} \left(p_j w_{ij} \sigma_j^{-2}\right)}{\sum_{i \neq j} \left(w_{ij} \sigma_j^{-2}\right)}$$

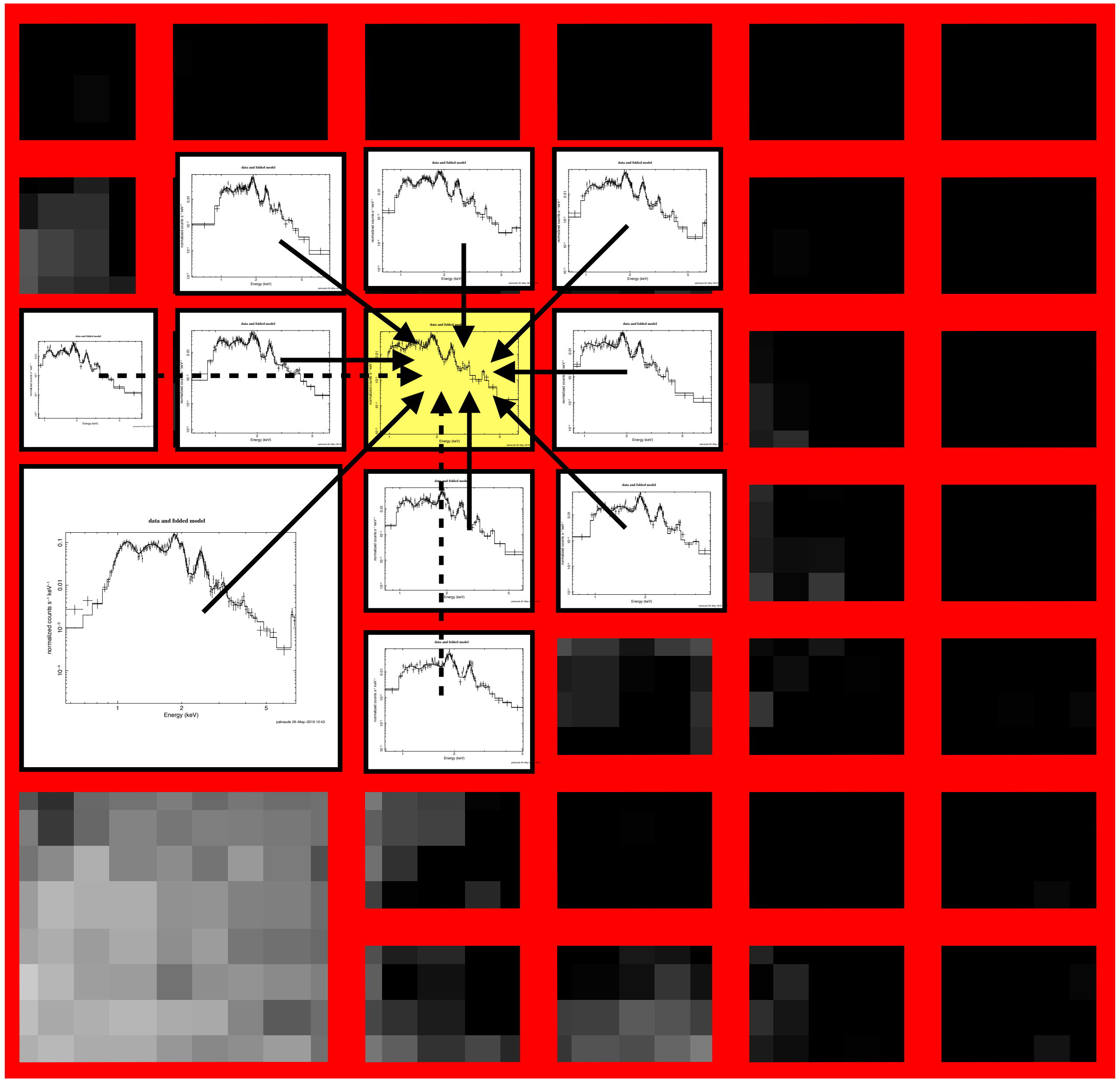

Schematic representation of how adjecent regions contribute to the initial spectral parameter estimates for the region in yellow

For each epoch from 2000 - 2018:

- pixels are selected using a Weighted Voroni Tesselation with S/N > 80 (> 1000 counts/region)
- due to the bulk expansion of Cas A, the region locations and number of regions are epoch dependent
- spectral parameters in any region are a convolution of the emission from that region and contributions from adjacent pixels
- use WVT mask to inform fitting parameters

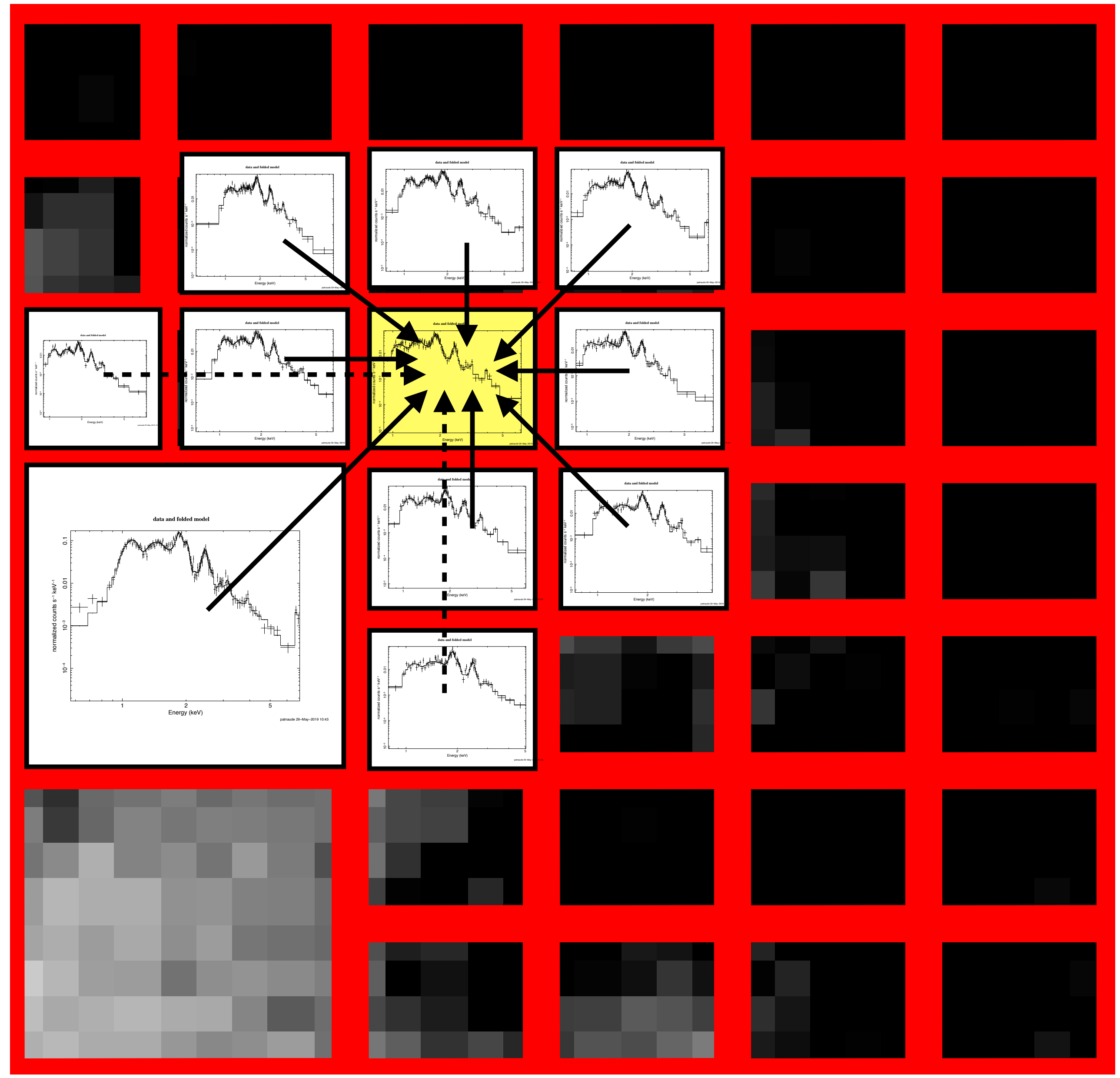

Schematic representation of how adjecent regions contribute to the initial spectral parameter estimates for the region in yellow

The process is iterated in order to minimize any error propagation due to local minima in the parameter χ^2 space and its effects on parameter estimation in adjacent pixels

Harvard-Smithsonian Center for Astrophysics

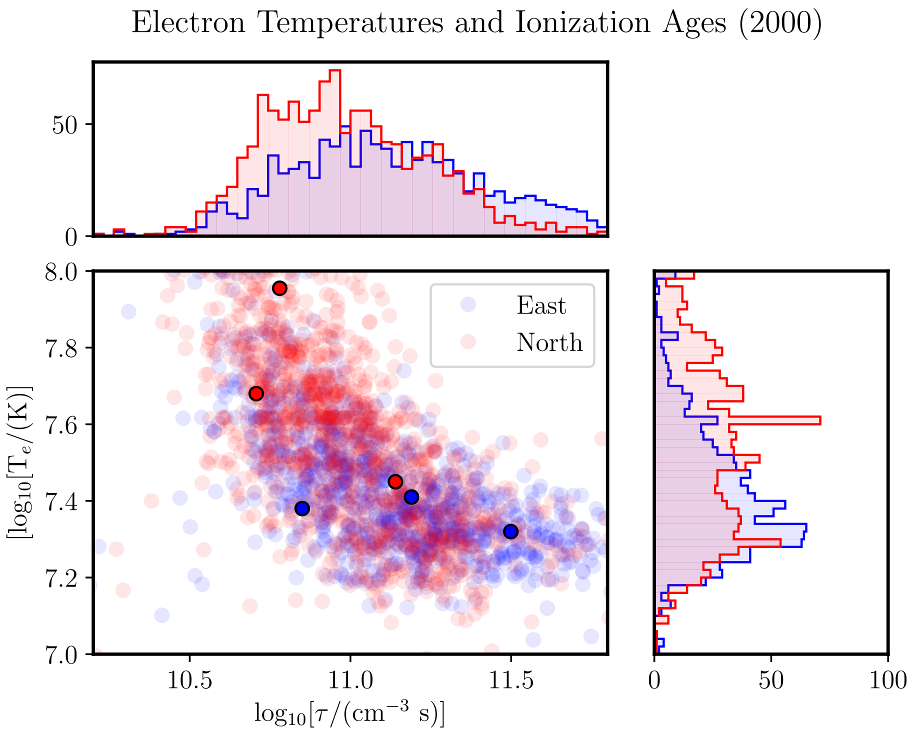

- Fits to each region produce a distribution of temperatures, ionization states, and chemical compositions
- Comparisons of the distribution of fit parameters from different cardinal directions highlight asymmetry in the SNR

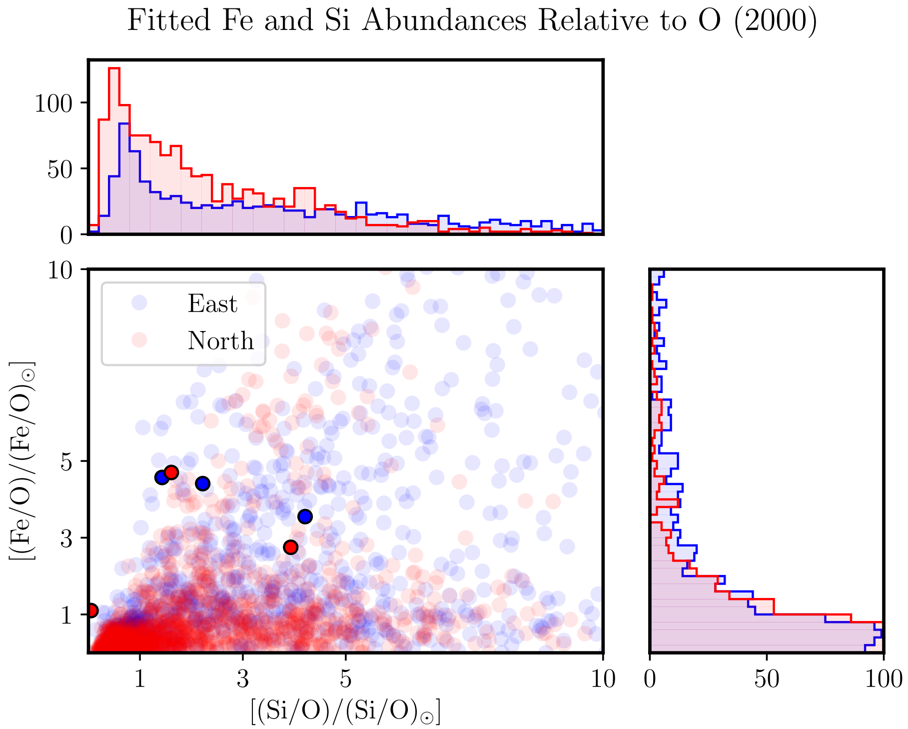

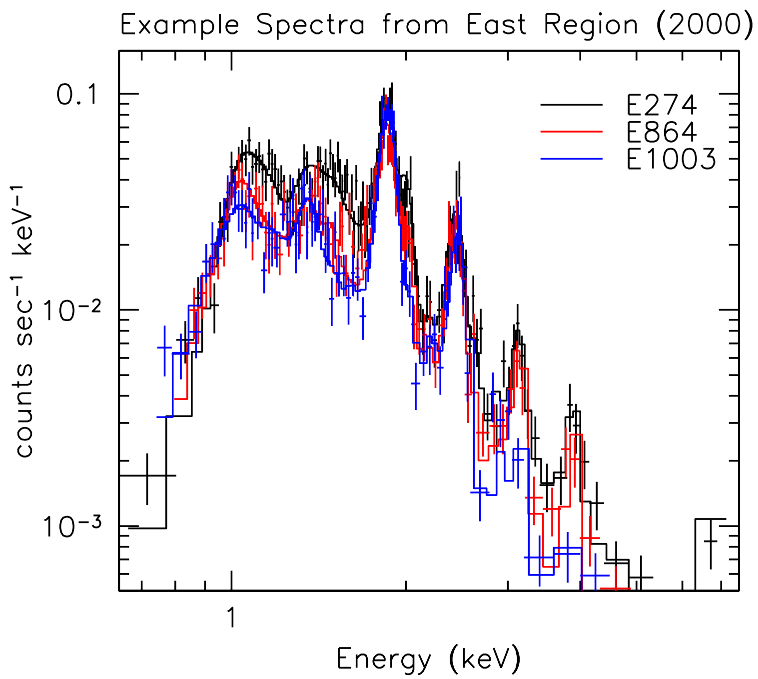

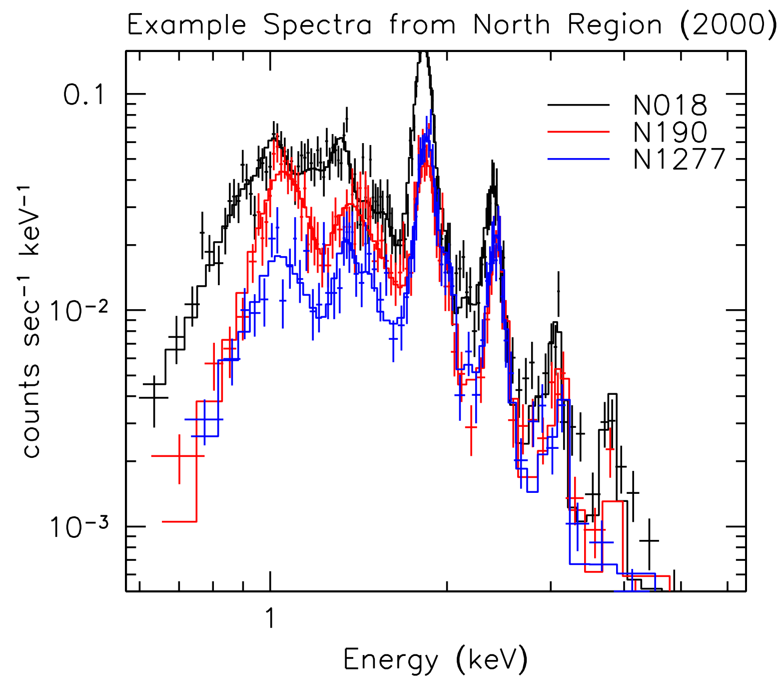

SNRs in Crete II

Dan Patnaude (SAO)

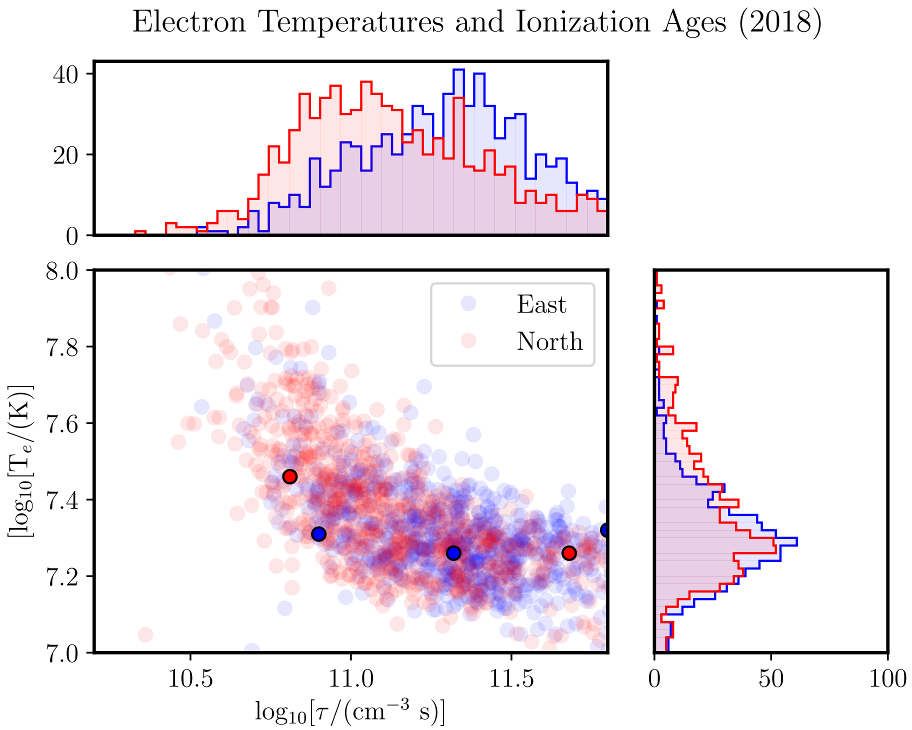

- Fits to each region produce a distribution of temperatures, ionization states, and chemical compositions
- Comparisons of the distribution of fit parameters from different cardinal directions highlight asymmetry in the SNR

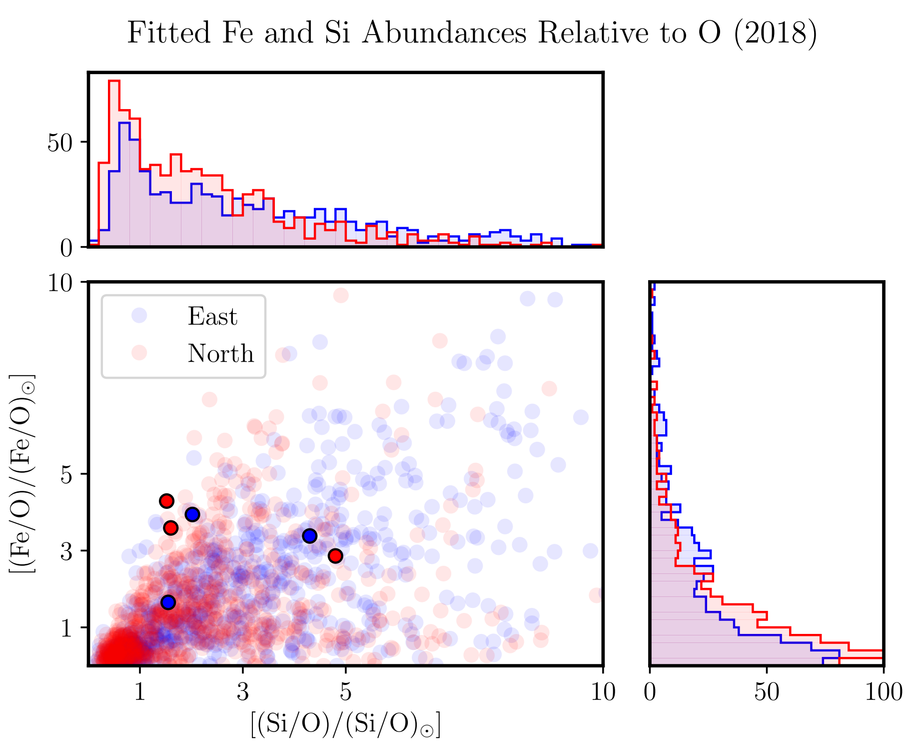

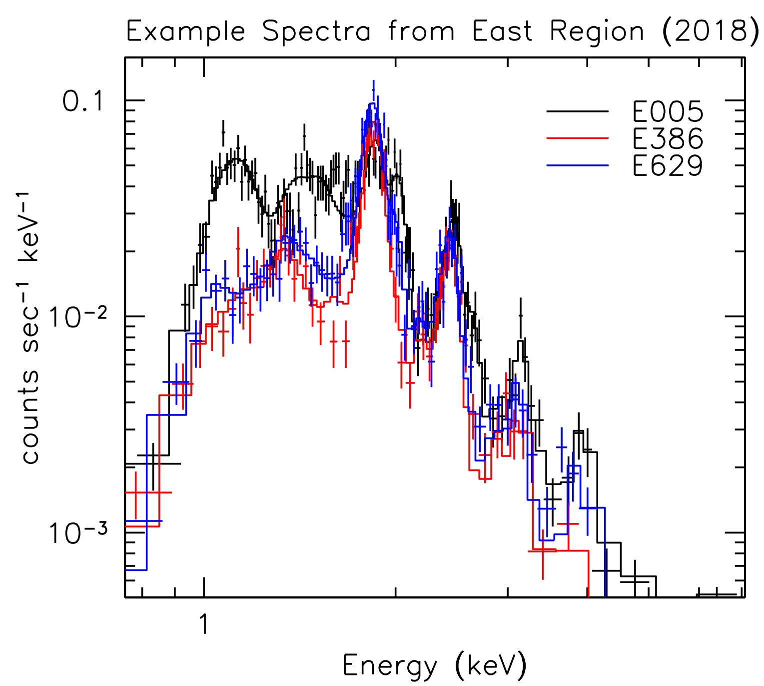

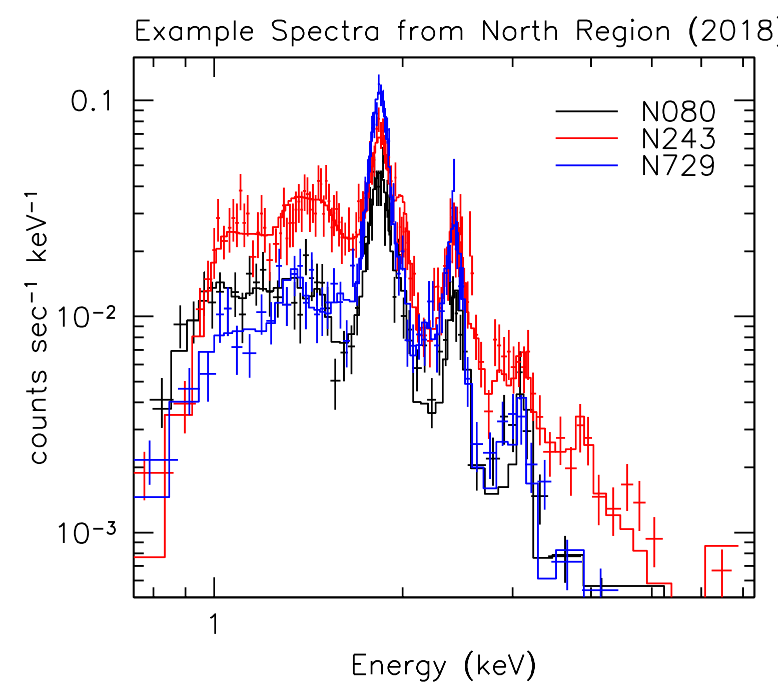

Quantitative Differences Between Regions

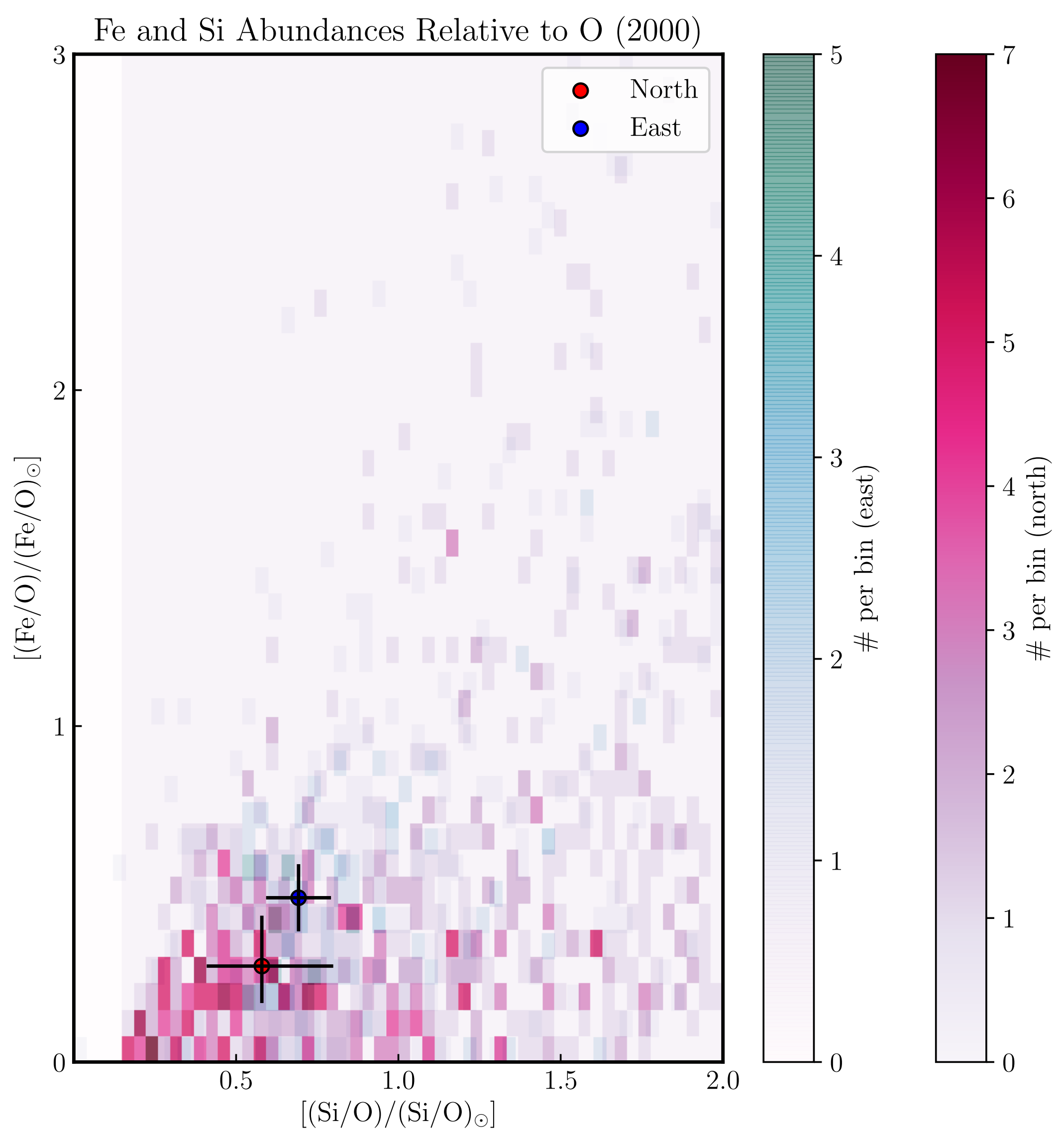

- In each region, abundances are fit relative to oxygen
- Fe/Si is generally higher in east than in north (~ 0.5)
- Results are broadly consistent with Laming & Hwang (2003) and $15M_{sun}$ progenitor models

Beyond larger scatter in 2018 dataset, no gross differences are seen in the abundances between 2000 and 2018

Quantitative Differences Between Regions

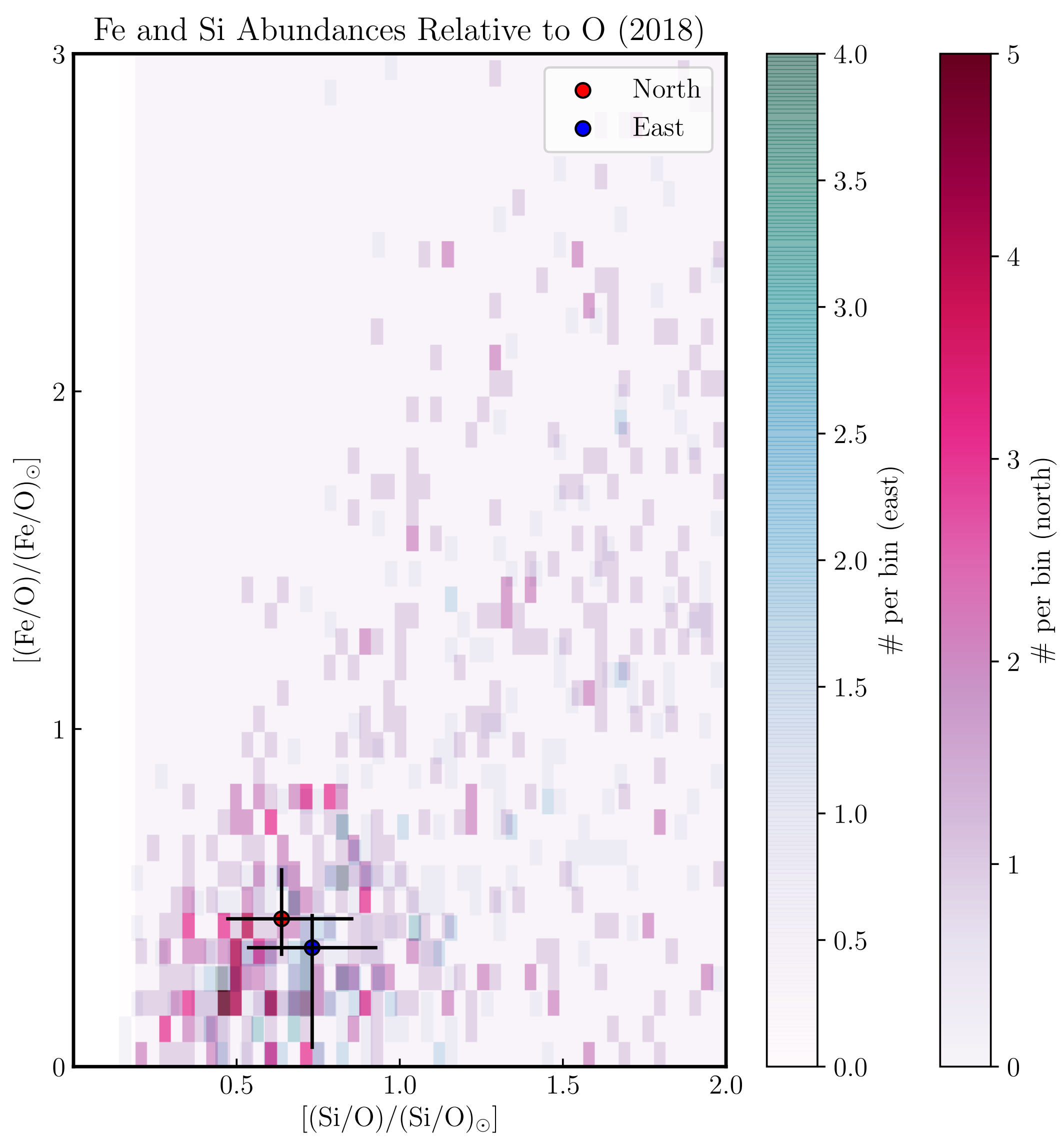

- In each region, abundances are fit relative to oxygen
- Fe/Si is generally higher in east than in north (~ 0.5)
- Results are broadly consistent with Laming & Hwang (2003) and $15M_{sun}$ progenitor models

Beyond larger scatter in 2018 dataset, no gross differences are seen in the abundances between 2000 and 2018

Quantitative Differences Between Regions

	T_e (keV)	$n_e t$ (10^{11} s cm^{-3})
2000	2,1	1,5
2018	1,7	2,4

- “k-means” test computes cluster averages from 2D distribution
- outliers can drag mean away from “best fit (by eye)”
- underlying kernel is dependent upon the explosion, composition, and circumstellar properties
- differences between epochs also reflect underlying adiabatic expansion of the SNR (Sato et al. 2017)

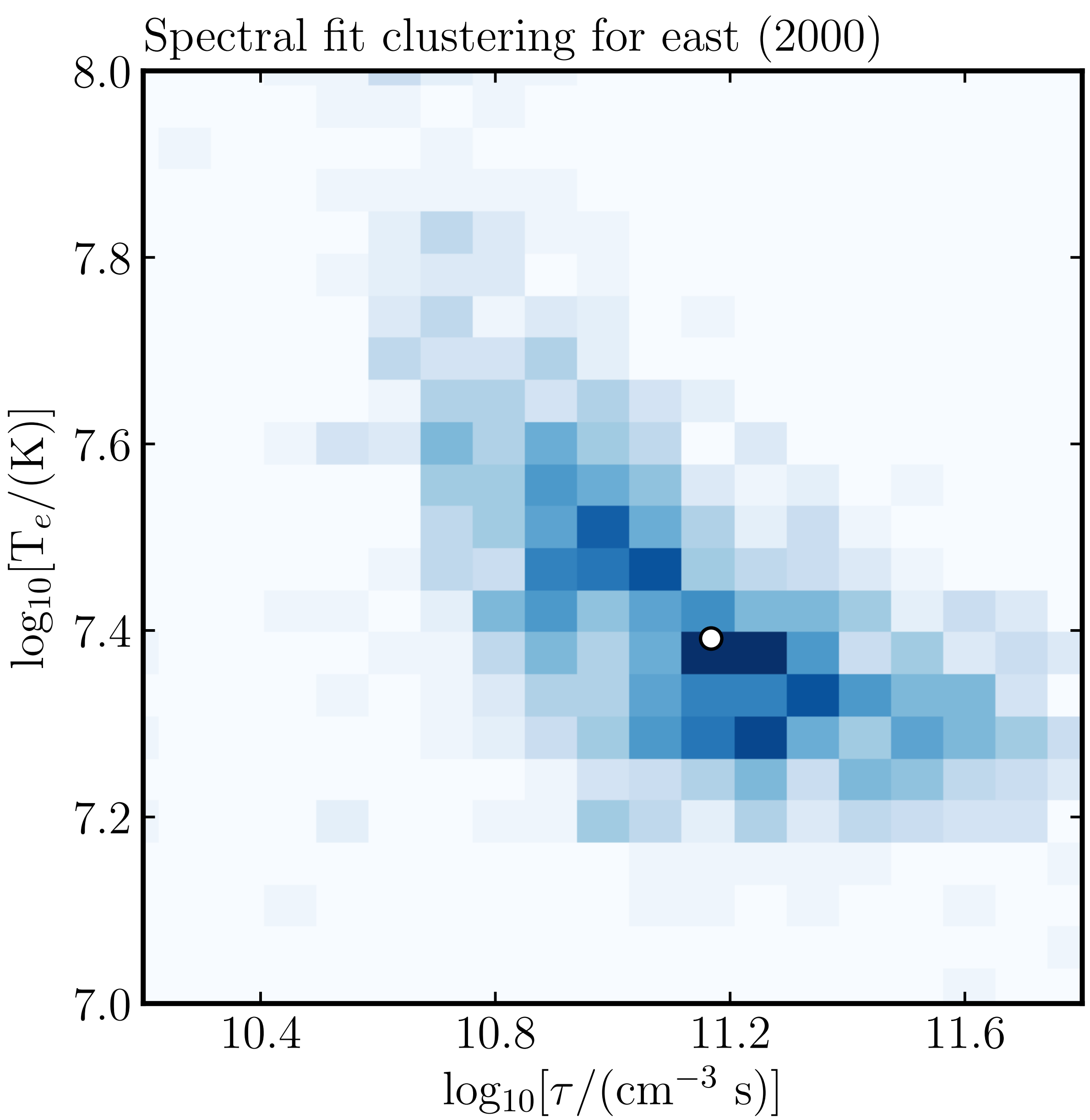

Quantitative Differences Between Regions

	T_e (keV)	$n_e t$ (10^{11} s cm^{-3})
2000	2,1	1,5
2018	1,7	2,4

- "k-means" test computes cluster averages from 2D distribution
- outliers can drag mean away from "best fit (by eye)"
- underlying kernel is dependent upon the explosion, composition, and circumstellar properties
- differences between epochs also reflect underlying adiabatic expansion of the SNR (Sato et al. 2017)

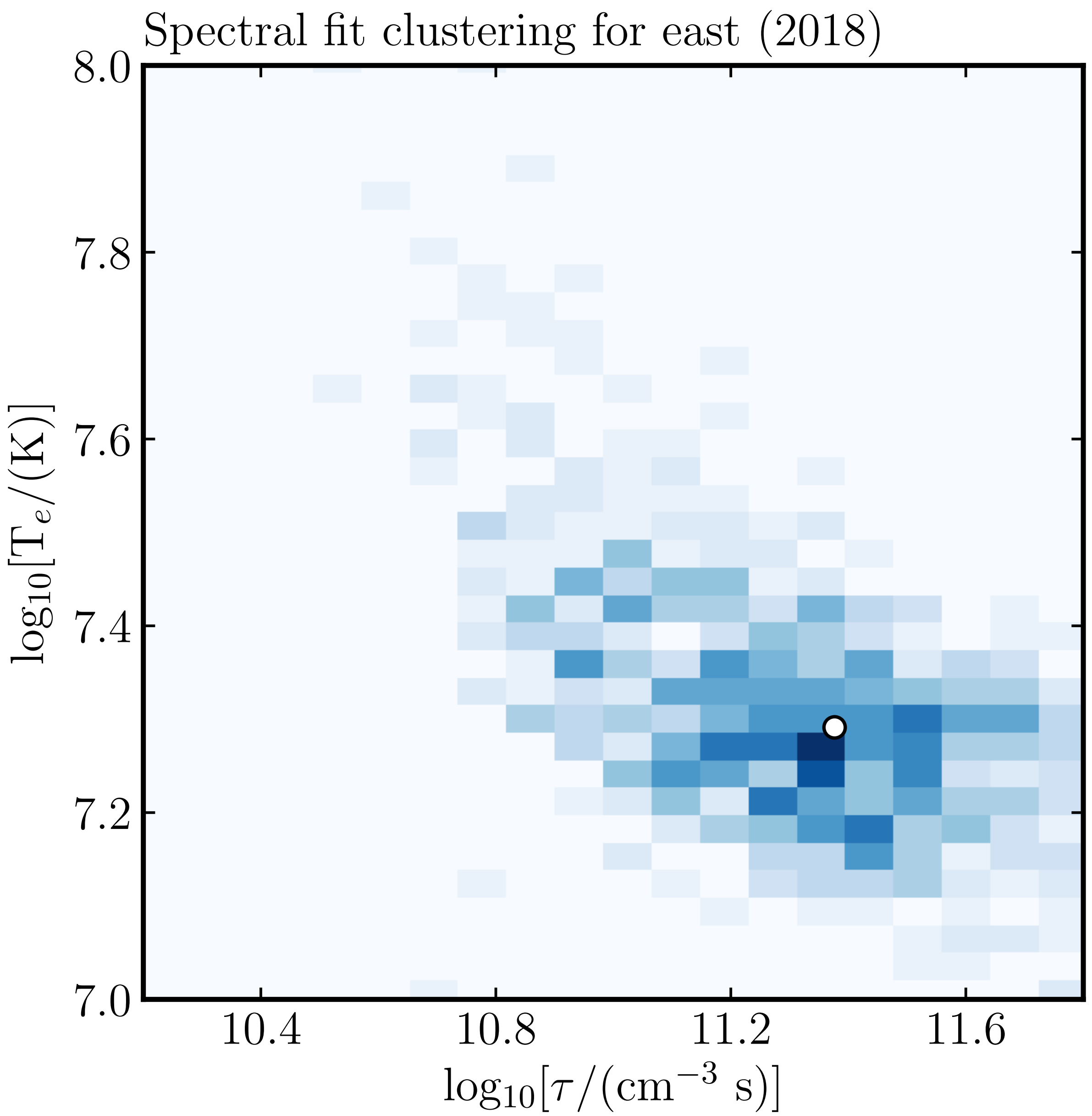

Quantitative Differences Between Regions

	T_e (keV)	n_et (10^{11} s cm^{-3})
2000	2,9	1,1
2018	1,9	1,6

- North region probably consists of more than one cluster

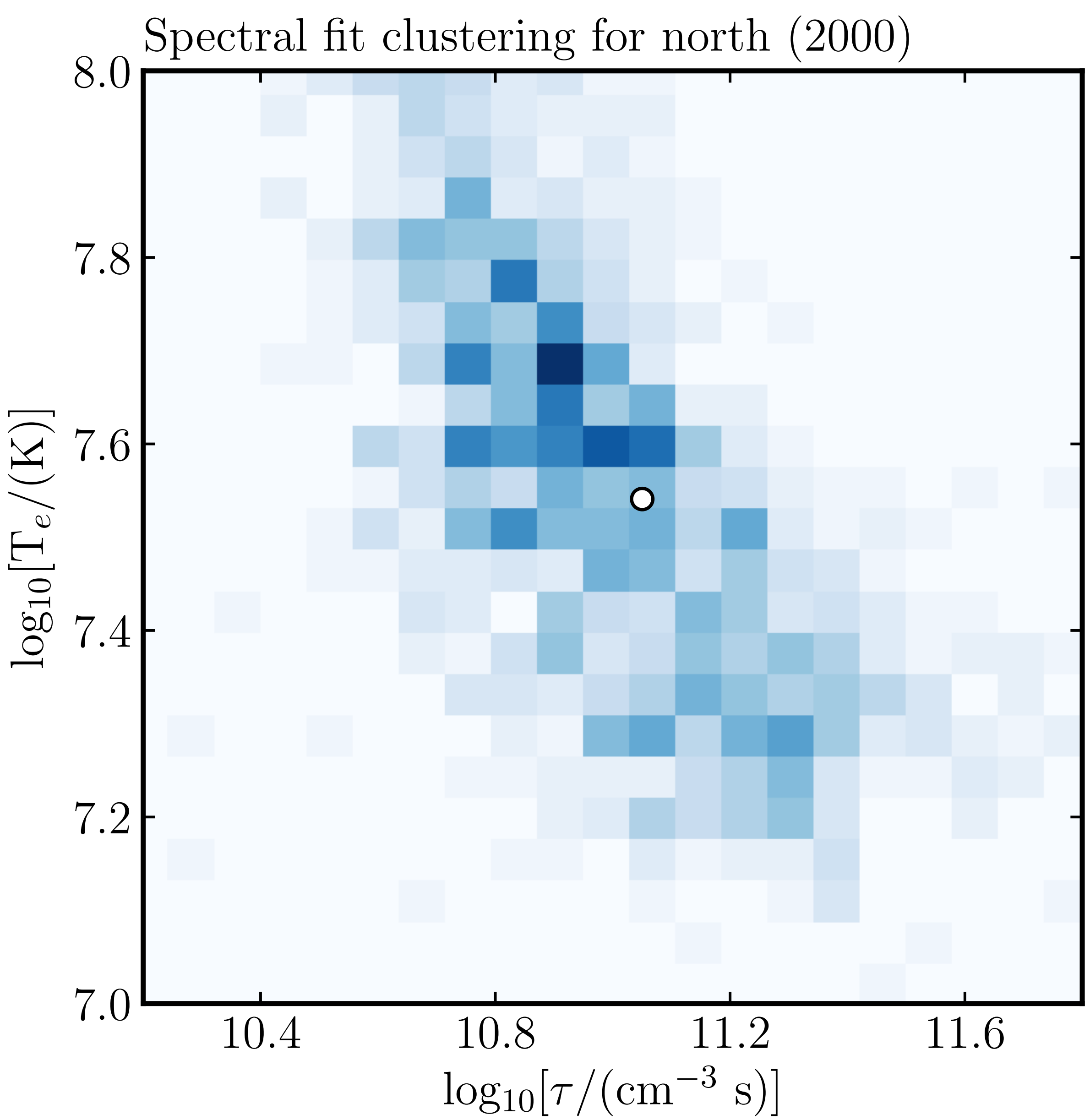

Quantitative Differences Between Regions

	T_e (keV)	$n_e t$ (10^{11} s cm^{-3})
2000	2,9	1,1
2018	1,9	1,6

- North region probably consists of more than one cluster

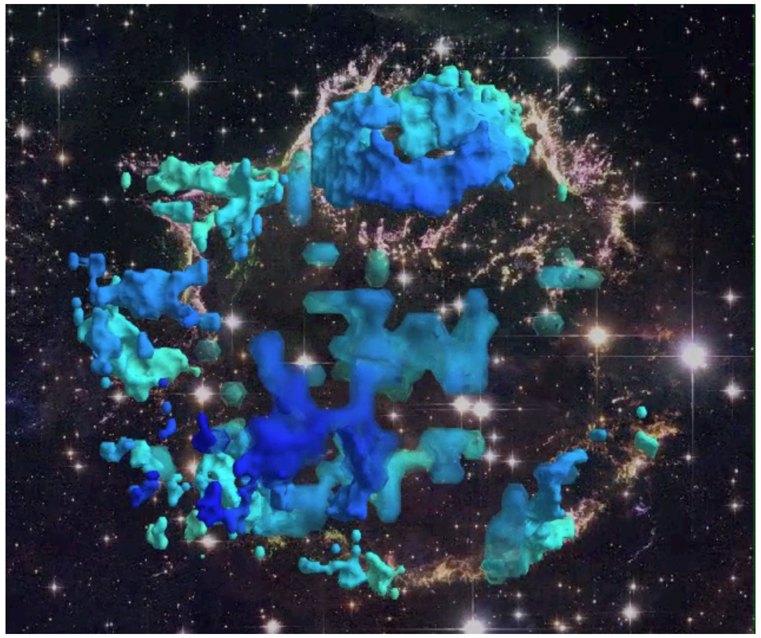

Milisavljevic & Fesen (2015)

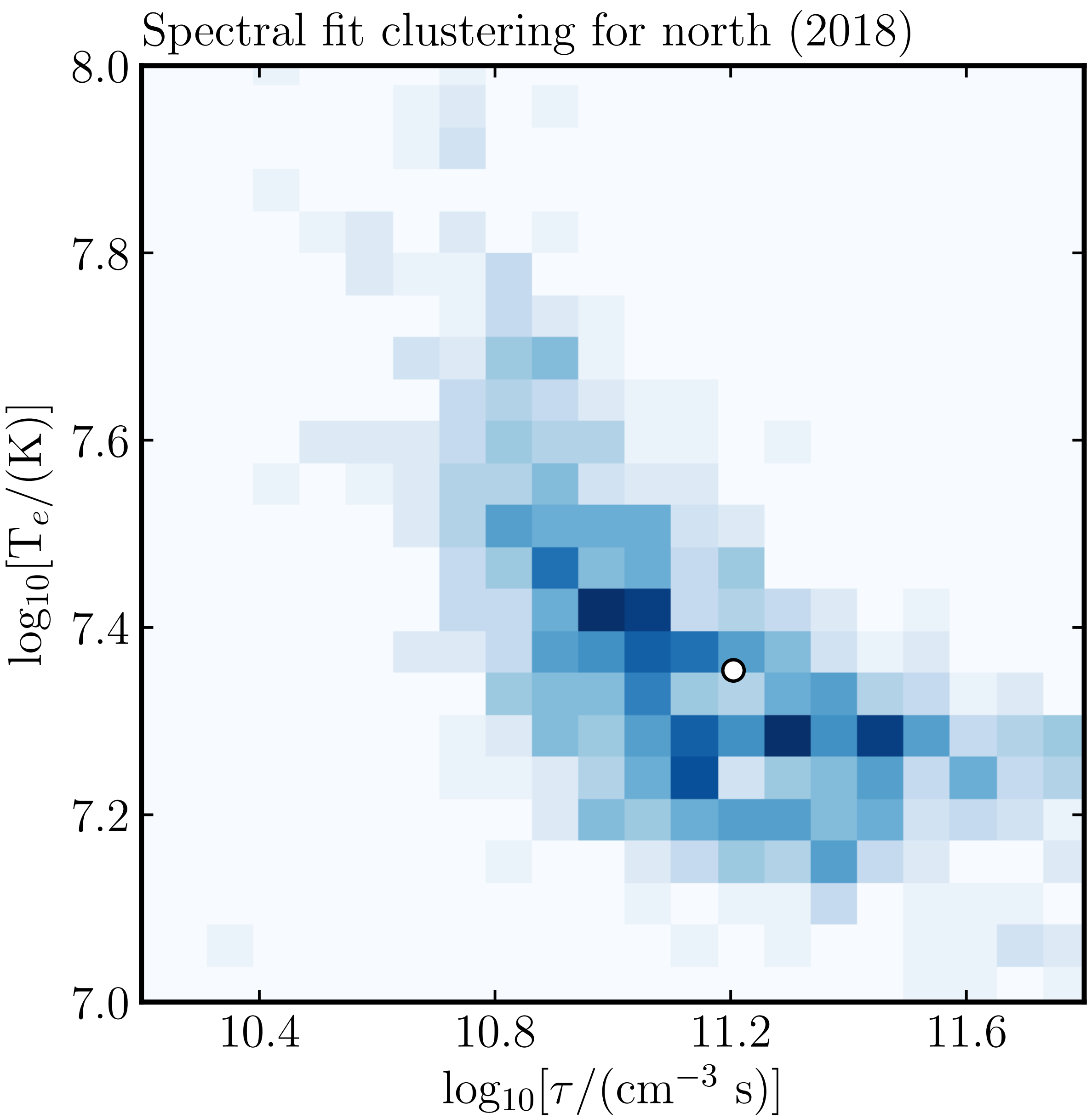

Quantitative Differences Between Regions

	T_e (keV)	$n_e t$ (10^{11} s cm^{-3})
2000	1,5	4,2
2018	1,5	3,2

- West region shows highest ionization ages
- In all, results are broadly consistent with results from Hwang and Laming
- changes in T_e and $n_e t$ can be compared against 3D models

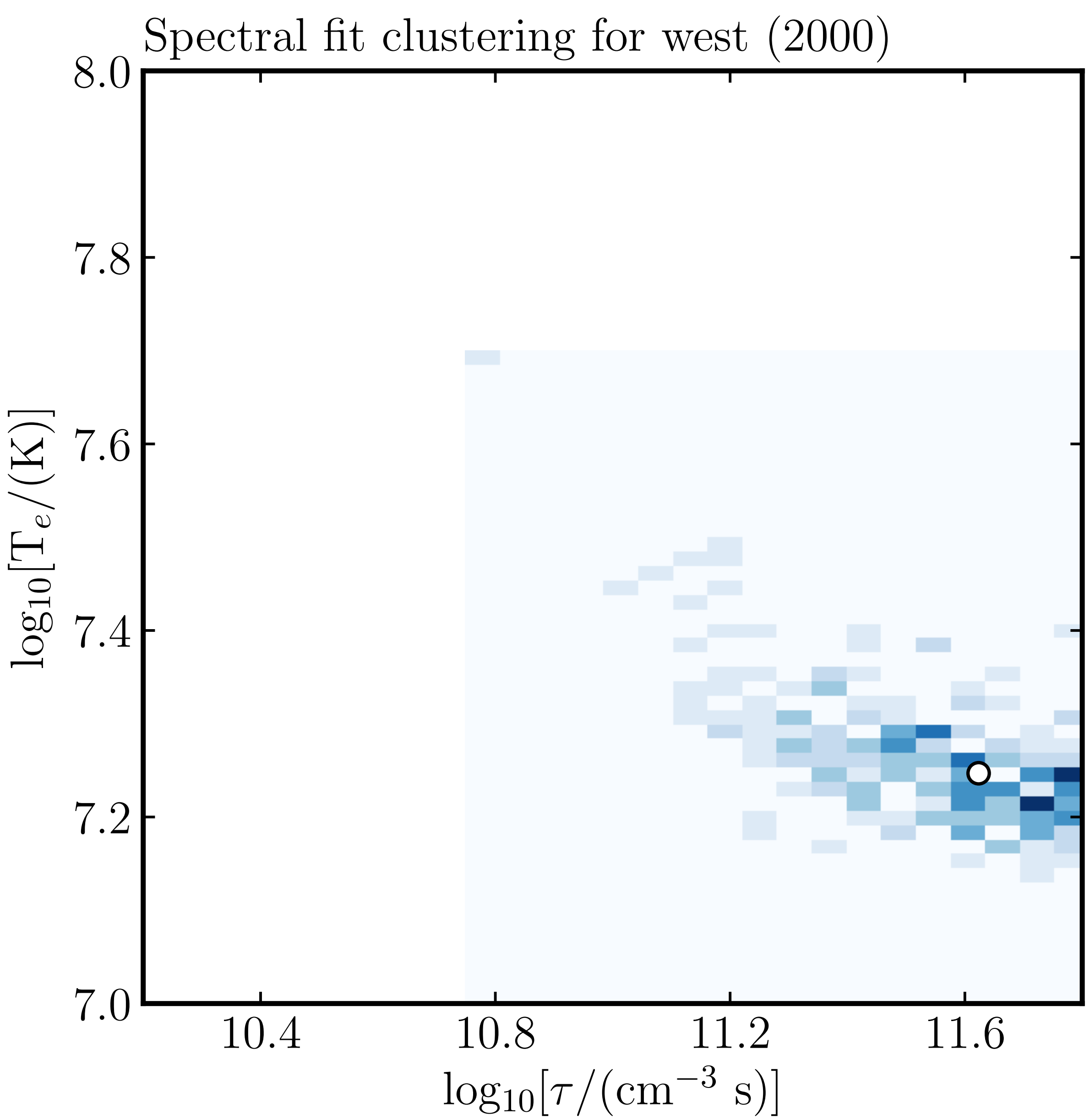

Quantitative Differences Between Regions

	T_e (keV)	$n_e t$ (10^{11} s cm^{-3})
2000	1,5	4,2
2018	1,5	3,2

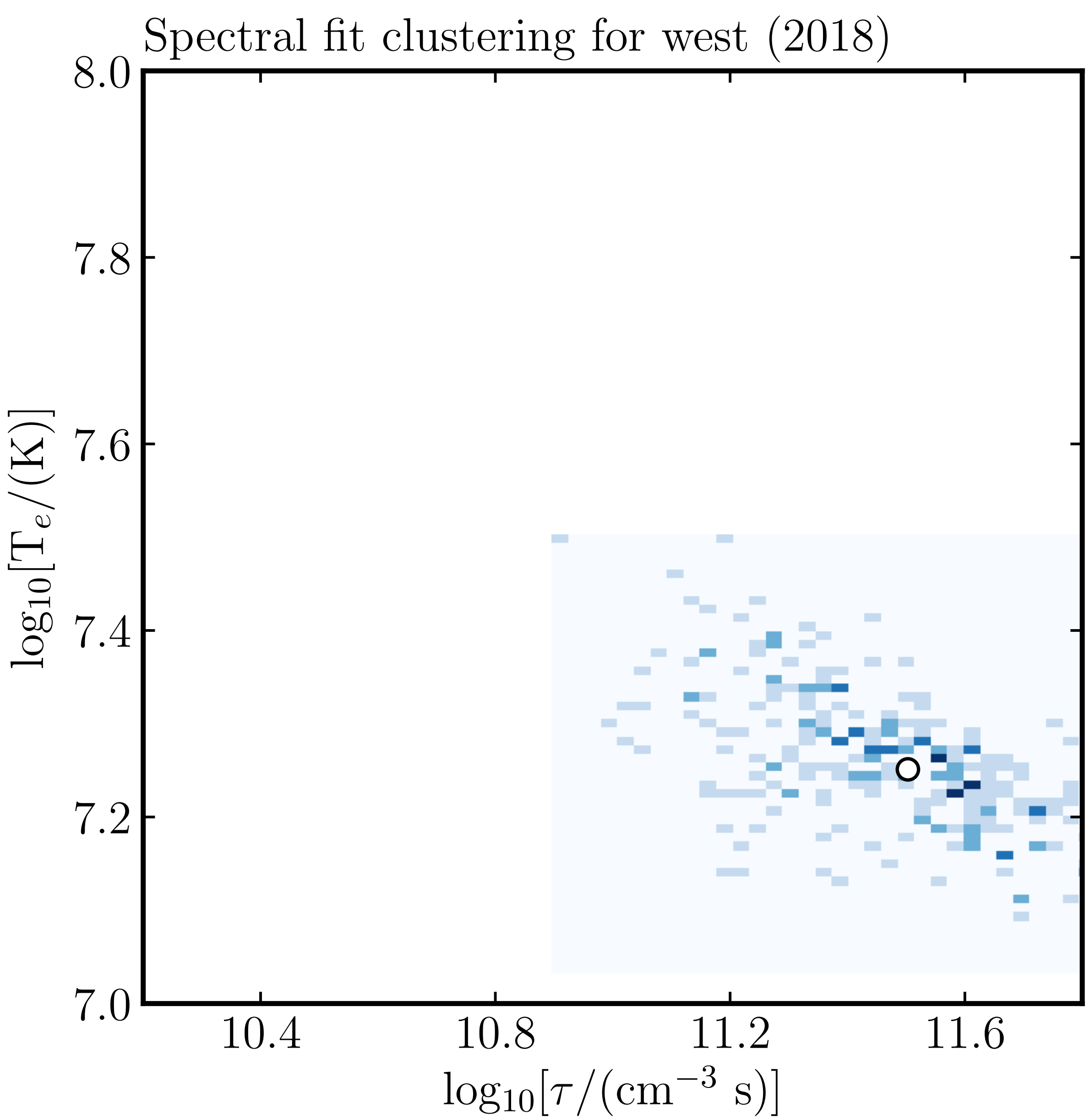

- West region shows highest ionization ages
- In all, results are broadly consistent with results from Hwang and Laming
- changes in T_e and $n_e t$ can be compared against 3D models

Comparisons to 1D Hydro Models

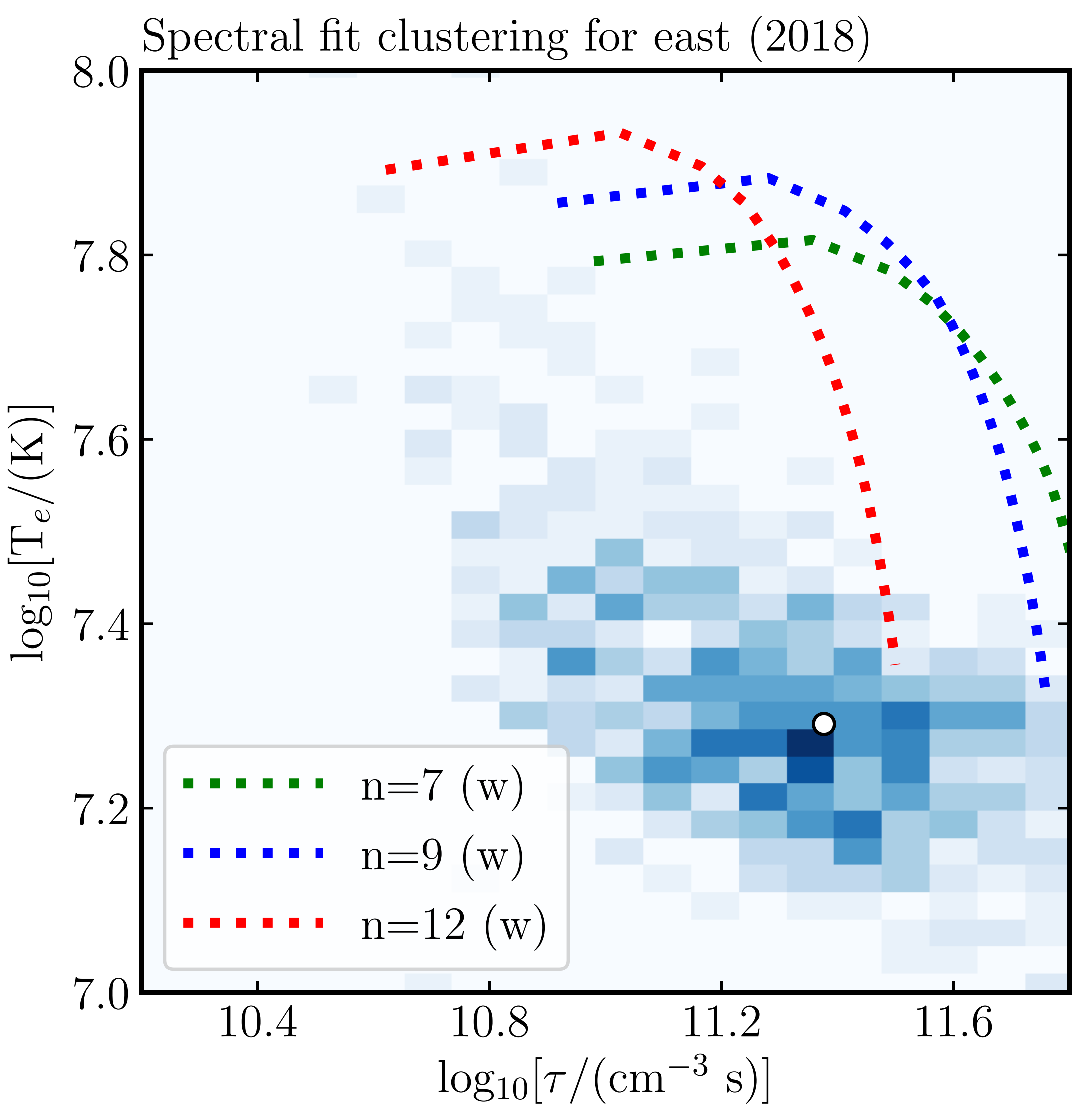

Model Cas A evolution to compare against the observed properties of the ejecta

$$\rho_{\rm CSM} = \frac{\dot{M}}{4\pi v_{\rm w} r^2} \left\{ \begin{array}{l} v_w = 15\ \mathrm{km\ s^{-1}} \\ \\ M_{dot} = 2\times10^{-5}\ M_{sun}\ \mathrm{yr^{-1}} \end{array} \right.$$

$$\rho_{\rm ej} \propto v^{-n}$$

$$\mathrm{M_{ej}} \approx 3\,\mathrm{M}_\odot$$

Use chemical composition from a model for SN 1993J, mapped onto a self-similar ejecta profile

$$\mathrm{E_{SN}} = 1.5 \times 10^{51}\ \mathrm{erg}$$

Comparisons to 1D Hydro Models

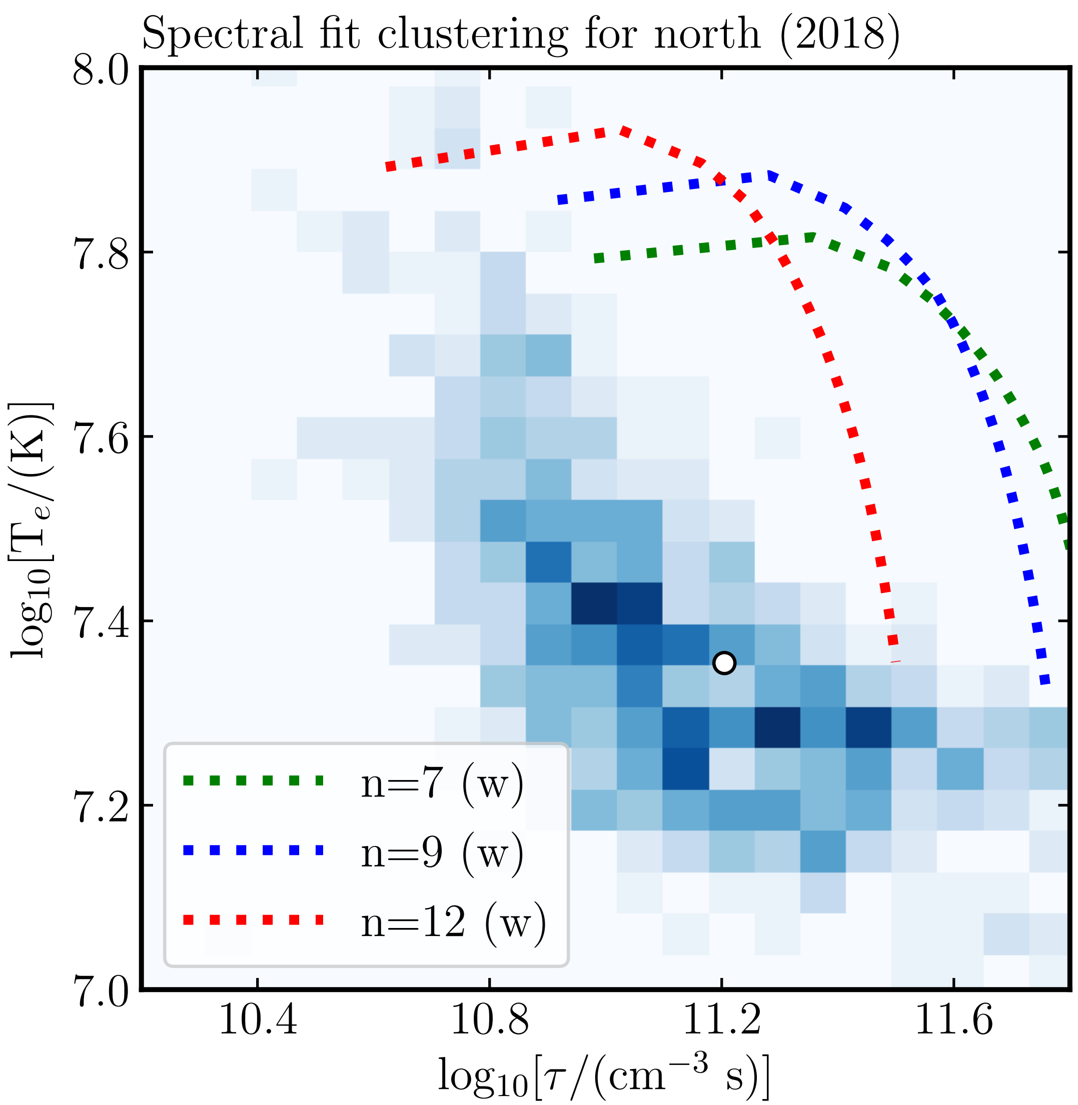

Model Cas A evolution to compare against the observed properties of the ejecta

ρ_C $\dot{M}$ $v_w = 15\ \mathrm{km\ s^{-1}}$ $(r > 0.2\ \mathrm{pc})$

$\mathrm{yr^{-1}}$

Ionization state and temperature of the ejecta are inconsistent with pure r^{-2} winds

$$\rho_{\mathrm{ej}} \propto v^{-n}$$

$$\mathrm{M_{ej}} \approx 3\,\mathrm{M_\odot}$$

$$\mathrm{E_{SN}} = 1.5 \times 10^{51}\ \mathrm{erg}$$

Use chemical composition from a model for SN 1993J, mapped onto a self-similar ejecta profile

Comparisons to 1D Hydro Models

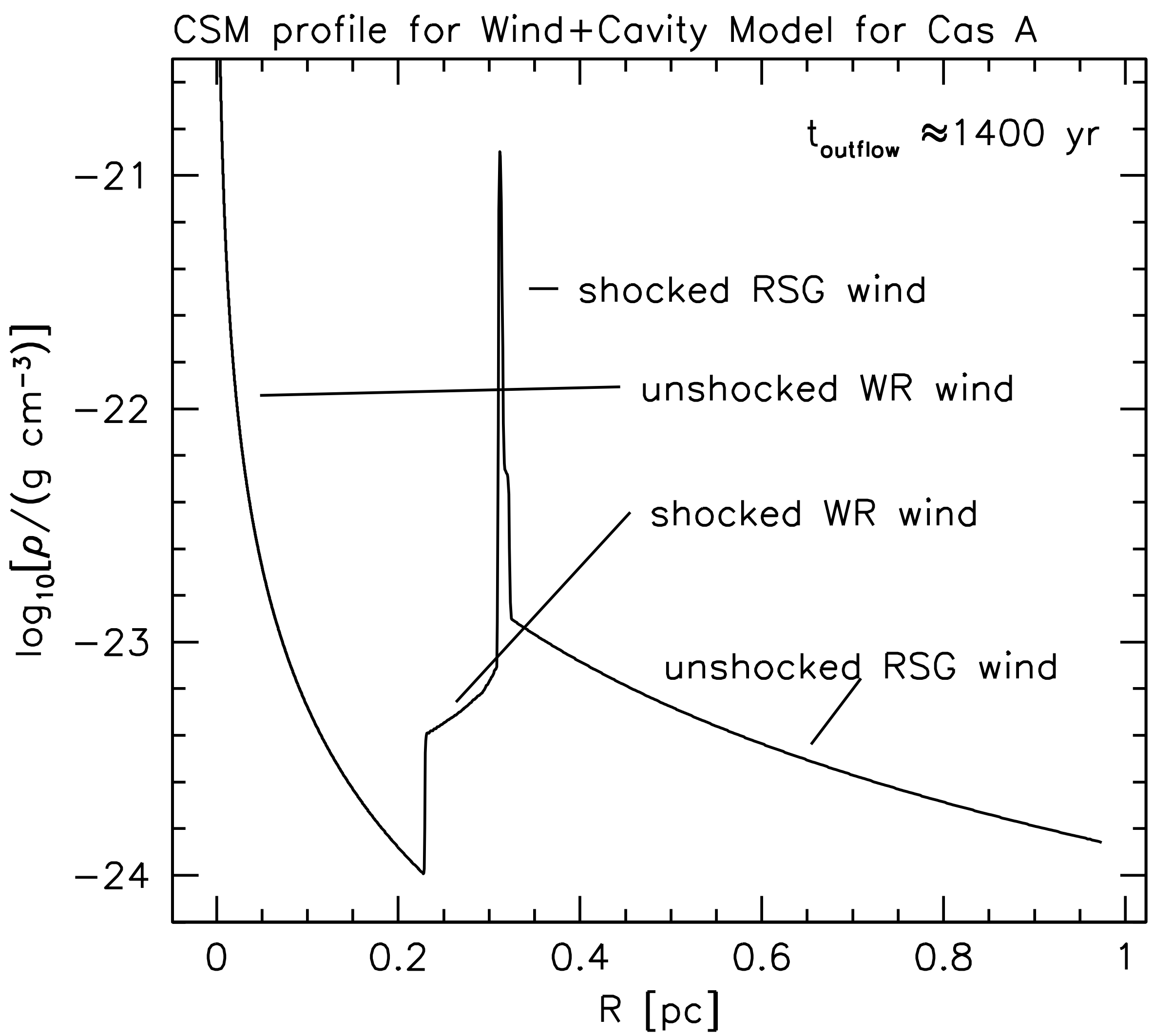

Possible CSM for Cas A progenitor

Model Cas A evolution to compare against the observed properties of the ejecta

$$\rho_{\rm CSM} = \frac{\dot{M}}{4\pi v_{\rm w} r^2}$$

- $v_w = 15$ km s^{-1} ($r > 0.2$ pc)
- **$v_w = 10^3$ km s^{-1} ($r < 0.2$ pc)**
- $M_{dot} = 2\times10^{-5}$ M_{sun} yr^{-1}

$$\rho_{\rm ej} \propto v^{-n}$$

$$\mathrm{M_{ej}} \approx 3\,\mathrm{M_\odot}$$

$$\mathrm{E_{SN}} = 1.5 \times 10^{51}\,\mathrm{erg}$$

Use chemical composition from a model for SN 1993J, mapped onto a self-similar ejecta profile

Comparisons to 1D Hydro Models

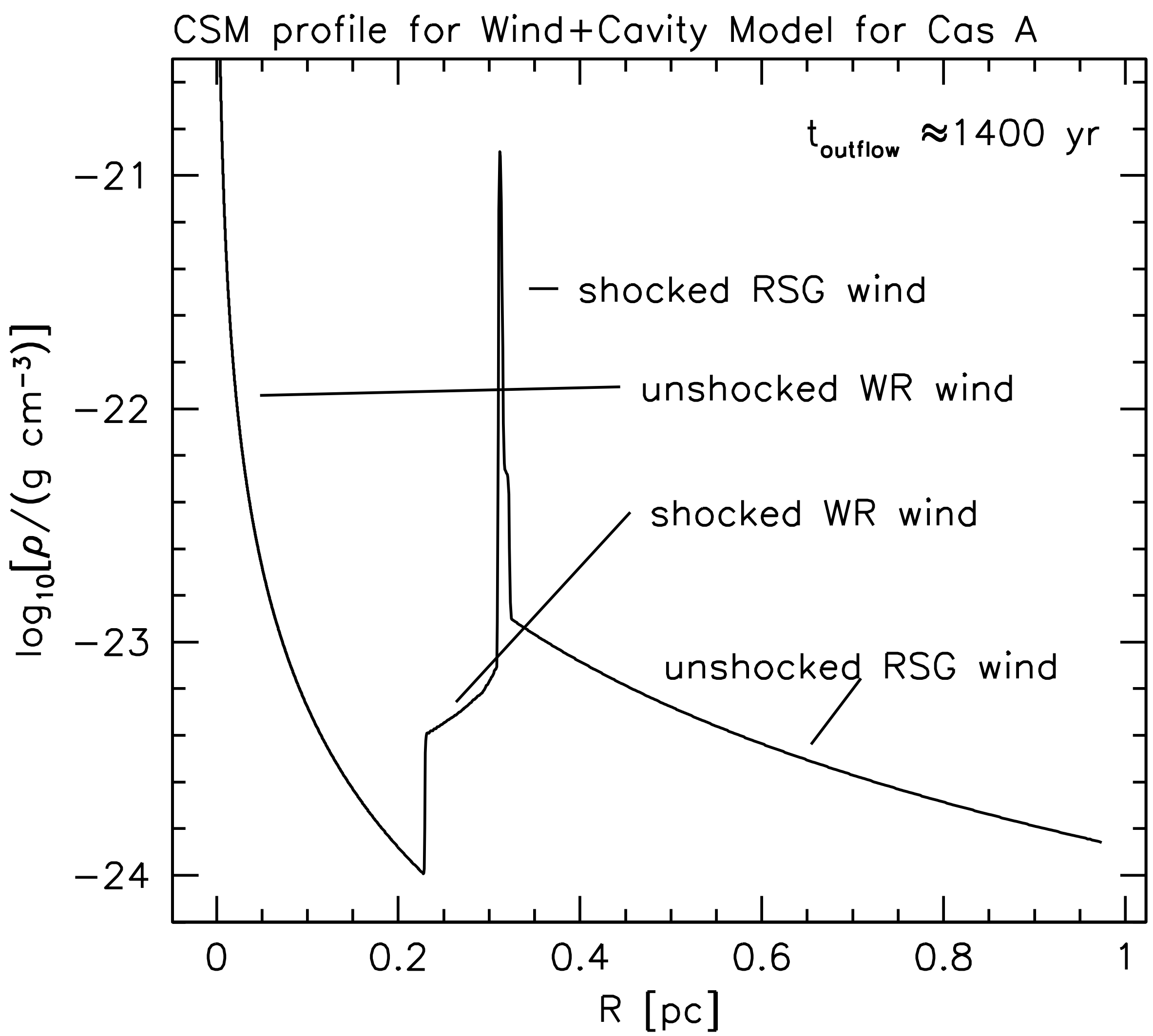

Possible CSM for Cas A progenitor

Model Cas A evolution to compare against the observed properties of the ejecta

n_{ej}	τ (10^{11} cm^{-3} s)	T_e (10^7 K)	R_{FS} pc	τ (10^{11} cm^{-3} s)	T_e (10^7 K)	R_{FS} pc
	Isotropic Wind[a]			Wind–Cavity[b]		
7	7.14	2.02	2.36	2.22	1.99	2.58
9	5.73	2.14	2.35	1.67	2.07	2.56
12	3.16	2.27	2.34	3.12	2.02	2.55

CSM models which include a small cavity produce larger SNR at 340 years, and generally lower ionization ages in the shocked ejecta

Comparisons to 1D Hydro Models

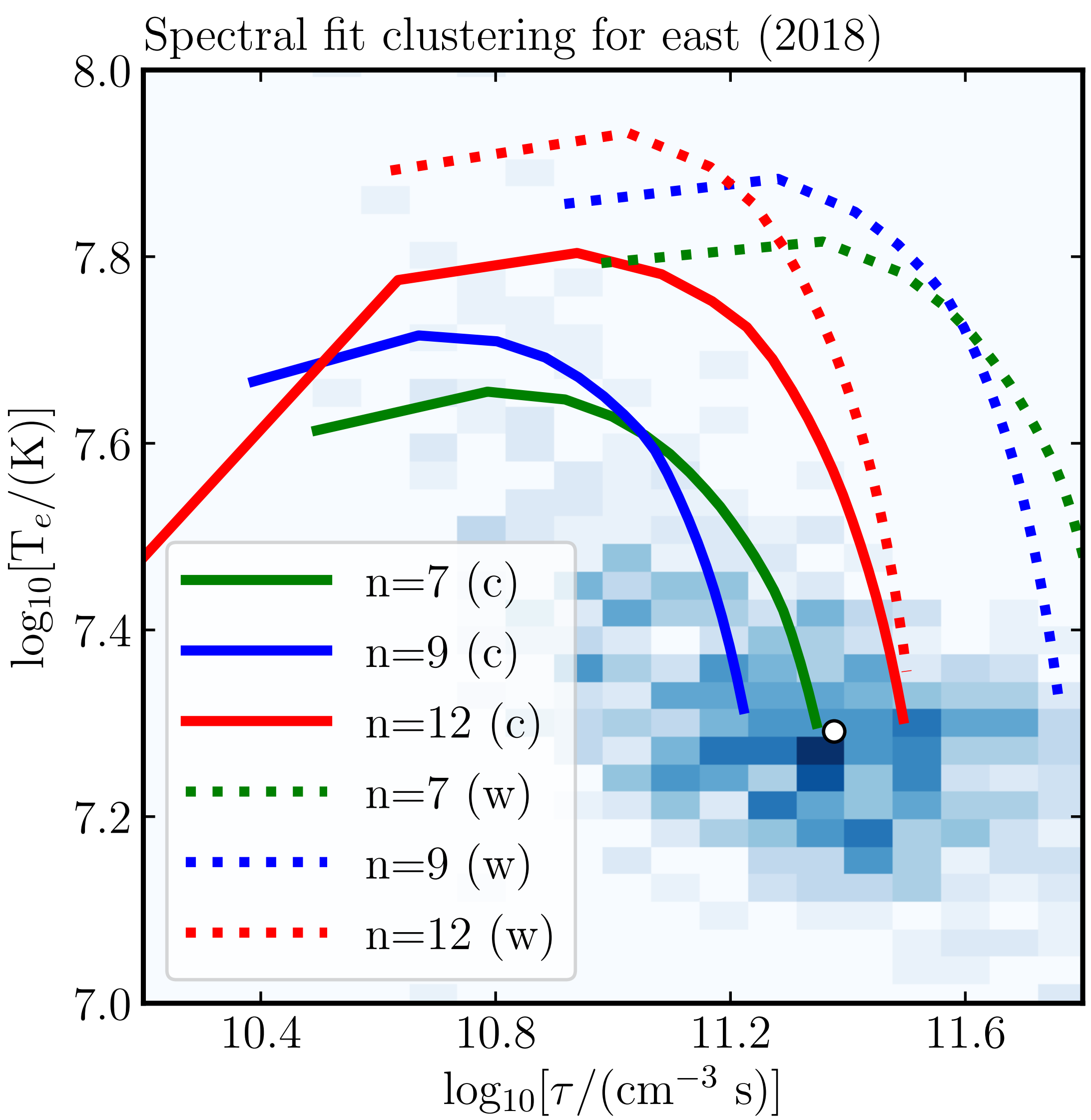

Model Cas A evolution to compare against the observed properties of the ejecta

$n_{\rm ej}$	τ (10^{11} cm^{-3} s)	T_e (10^7 K)	R_{FS} pc	τ (10^{11} cm^{-3} s)	T_e (10^7 K)	R_{FS} pc
	Isotropic Wind[a]			Wind–Cavity[b]		
7	7.14	2.02	2.36	2.22	1.99	2.58
9	5.73	2.14	2.35	1.67	2.07	2.56
12	3.16	2.27	2.34	3.12	2.02	2.55

CSM models which include a small cavity produce larger SNR at 340 years, and generally lower ionization ages in the shocked ejecta

Comparisons to 1D Hydro Models

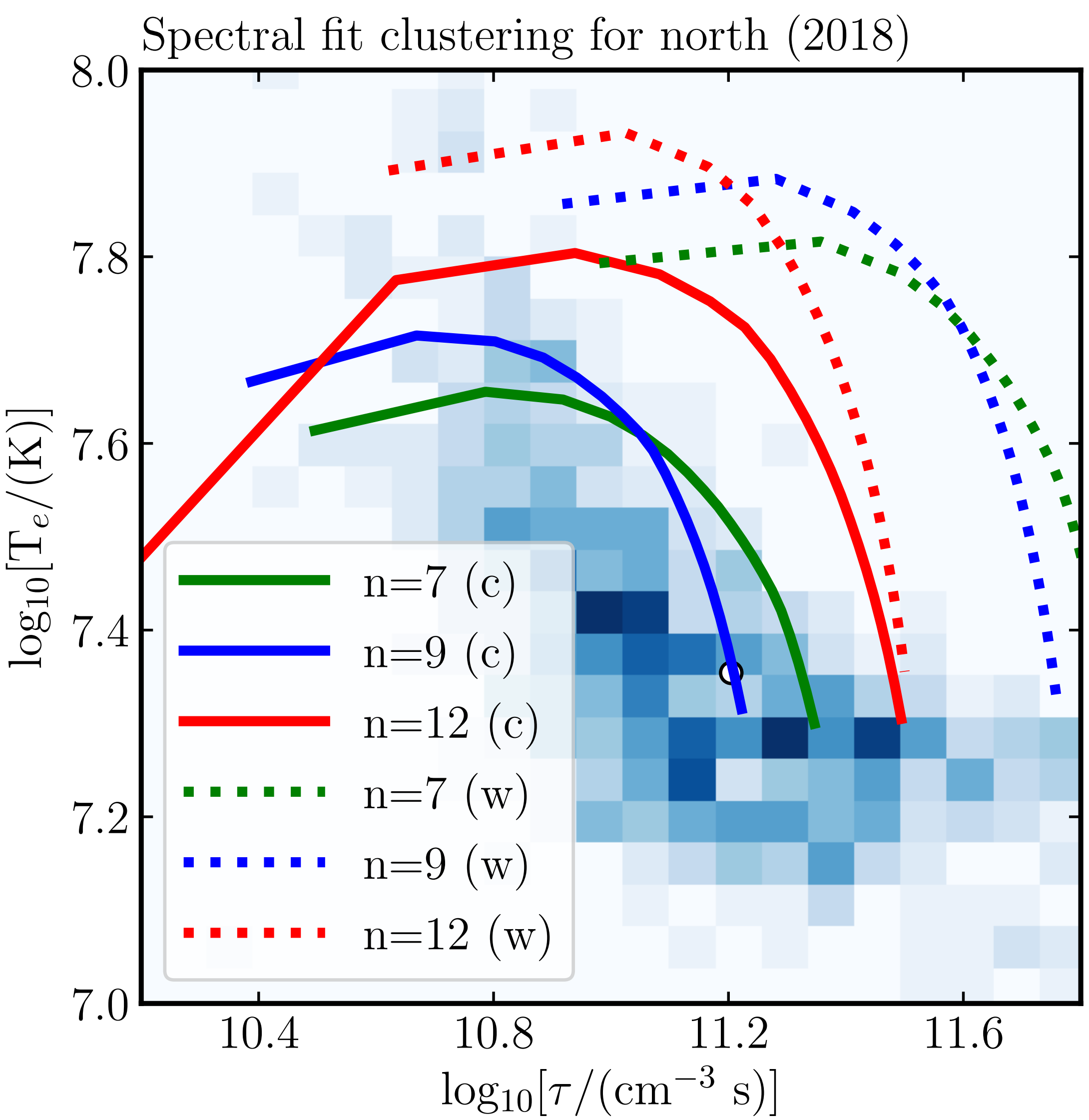

Model Cas A evolution to compare against the observed properties of the ejecta

n_{ej}	τ (10^{11} cm^{-3} s)	T_e (10^7 K)	R_{FS} pc	τ (10^{11} cm^{-3} s)	T_e (10^7 K)	R_{FS} pc
	Isotropic Wind[a]			Wind–Cavity[b]		
7	7.14	2.02	2.36	2.22	1.99	2.58
9	5.73	2.14	2.35	1.67	2.07	2.56
12	3.16	2.27	2.34	3.12	2.02	2.55

CSM models which include a small cavity produce larger SNR at 340 years, and generally lower ionization ages in the shocked ejecta

Comparisons to 1D Hydro Models

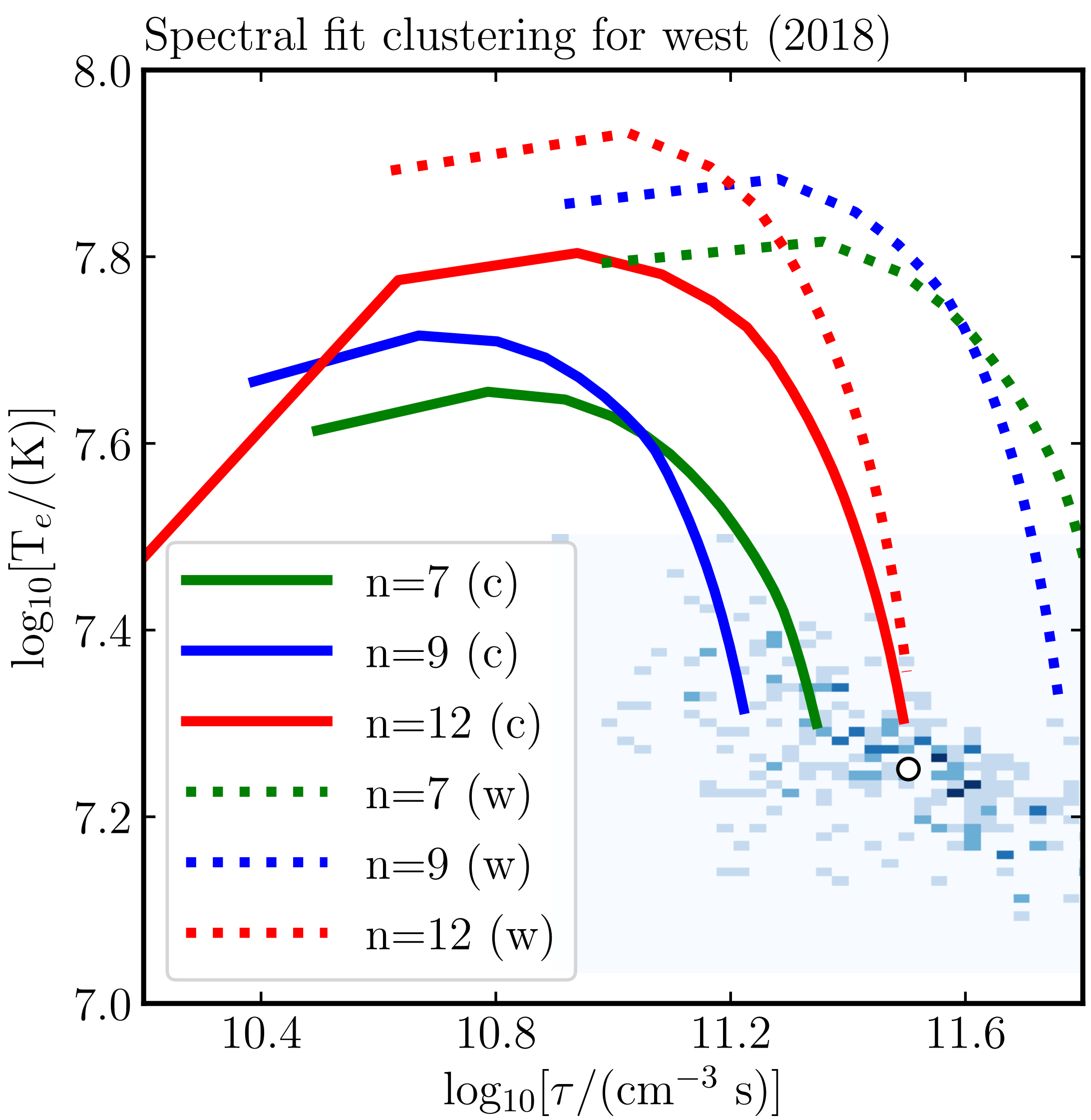

Model Cas A evolution to compare against the observed properties of the ejecta

n_{ej}	τ (10^{11} cm^{-3} s)	T$_e$ (10^7 K)	R$_{FS}$ pc	τ (10^{11} cm^{-3} s)	T$_e$ (10^7 K)	R$_{FS}$ pc
	Isotropic Wind[a]			Wind–Cavity[b]		
7	7.14	2.02	2.36	2.22	1.99	2.58
9	5.73	2.14	2.35	1.67	2.07	2.56
12	3.16	2.27	2.34	3.12	2.02	2.55

CSM models which include a small cavity produce larger SNR at 340 years, and generally lower ionization ages in the shocked ejecta

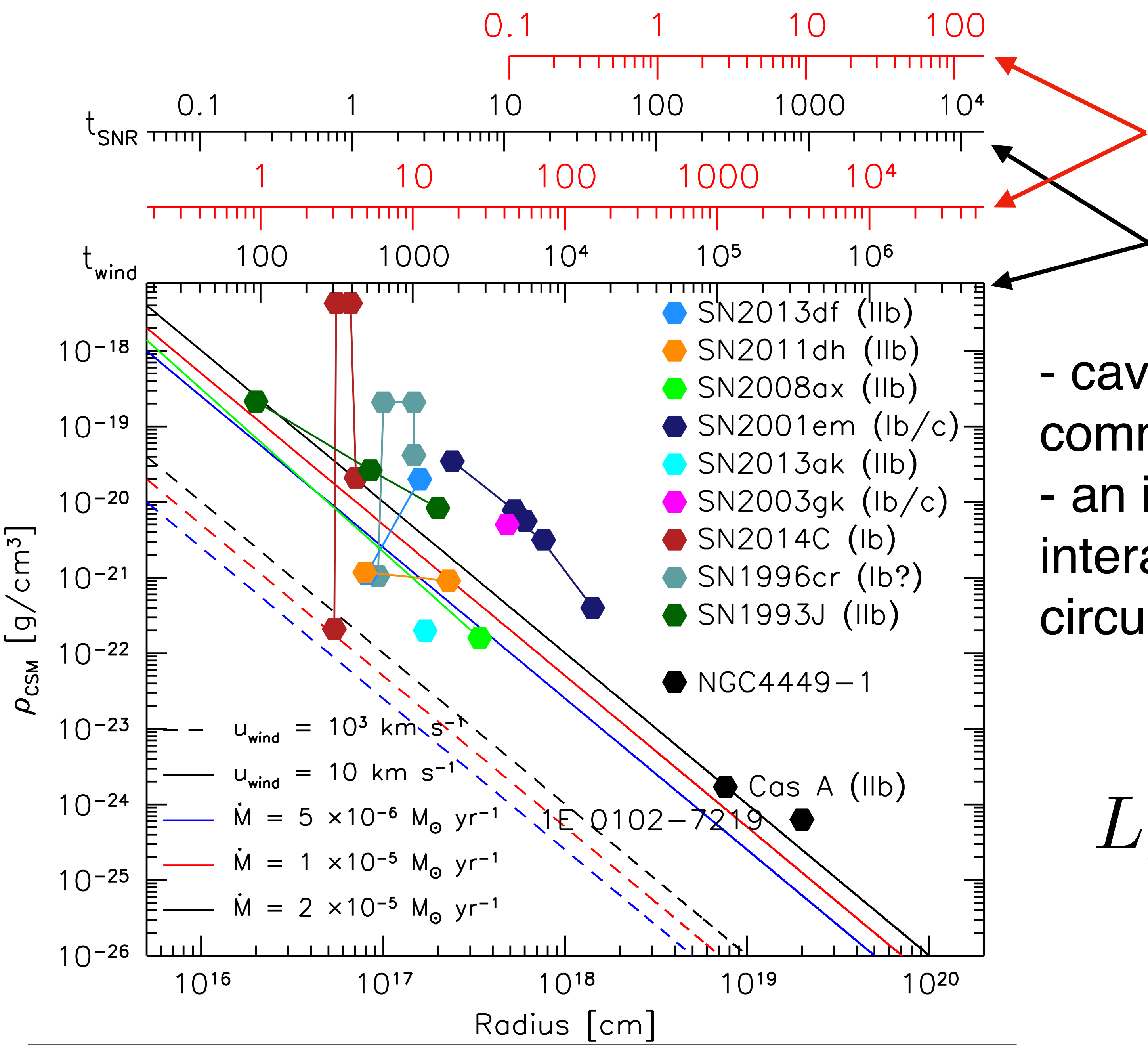

$v_{wind} = 10^3$ km s^{-1}

$v_{wind} = 10$ km s^{-1}

CSM properties for several Ib/c and IIb SNe and SNR

- cavities around IIb and Ib/c SNe appear to be common
- an increase in X-ray emission signals the interaction between the shock and denser circumstellar material

$$L_X = \left(\frac{4}{\pi \bar{m}^2}\right)\left(\frac{\dot{M}}{v_w}\right)\frac{\Lambda(T)}{R_s}$$

data from: Dwarkadas & Gruszko (2012); Margutti et al. (2017); Kundu et al. (2019); Patnaude et al. (2019, in prep); Milisavljevic & Fesen (2008); Lee et al. (2014); Xi et al. (2019)

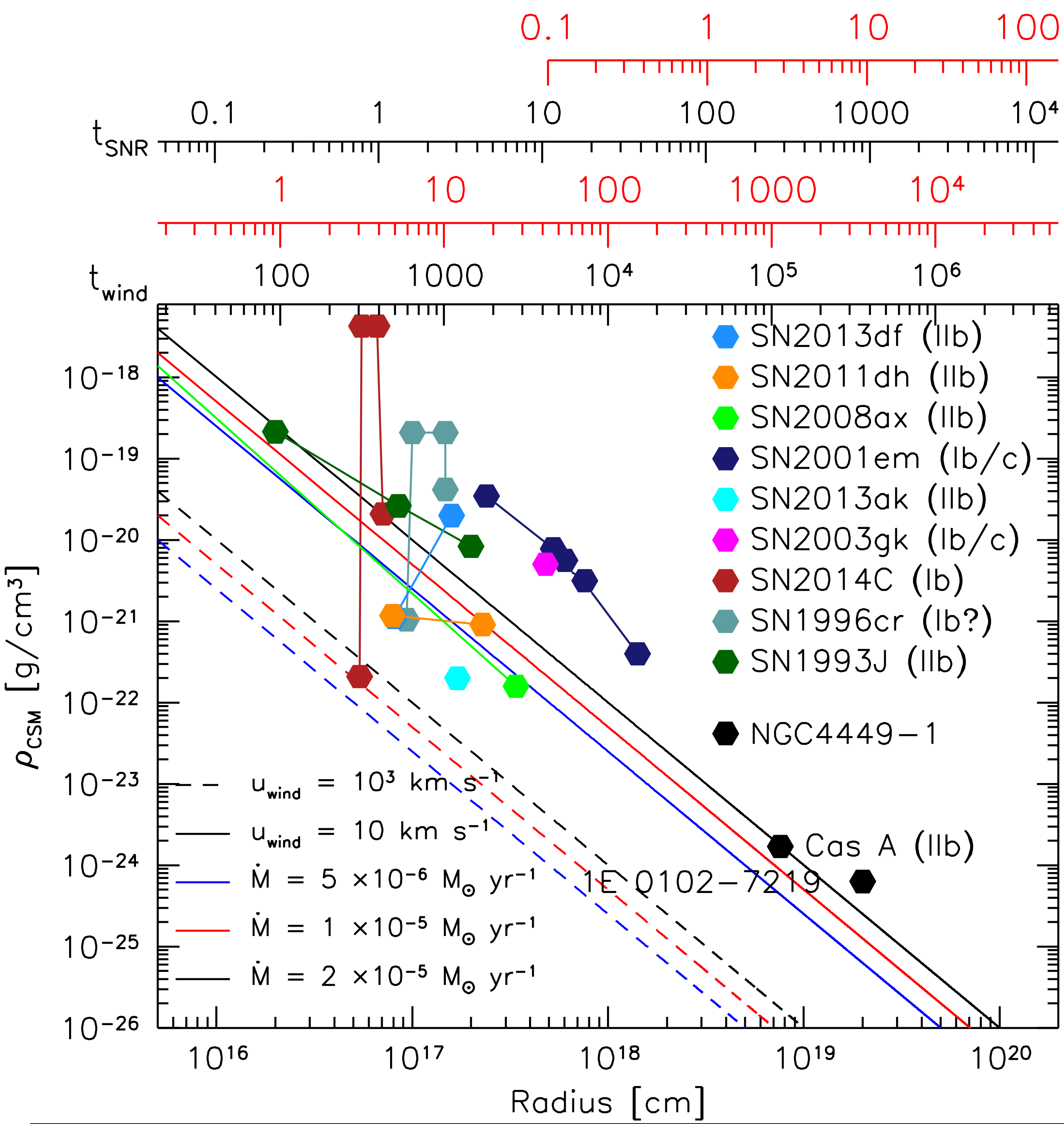

v_{wind} = 10^3 km s^{-1}

v_{wind} = 10 km s^{-1}

CSM properties for several Ib/c and IIb SNe and SNR

- cavities around IIb and Ib/c SNe appear to be common
- an increase in X-ray emission signals the interaction between the shock and denser circumstellar material

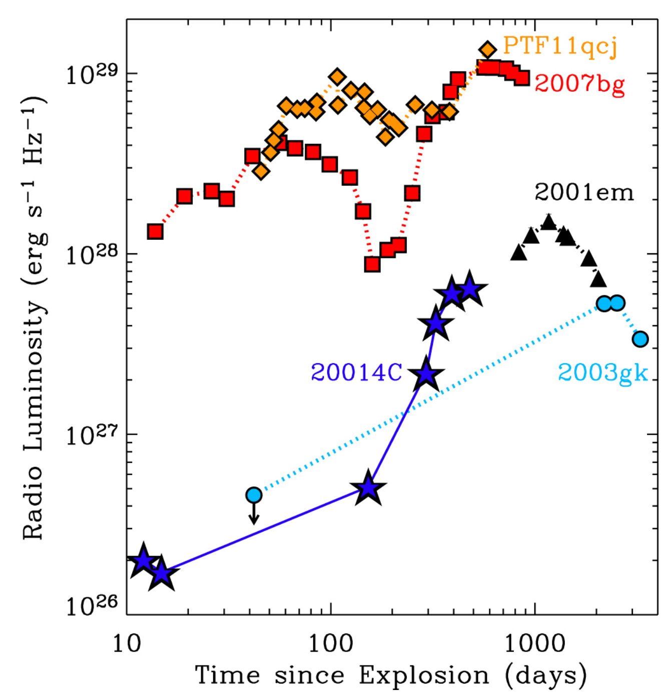

Margutti et al. (2017)

SN 2003gk:

$$L_X \approx 1.7 \times 10^{39}\,\mathrm{erg\,s^{-1}}$$

$$\rightarrow \dot{M} \approx 0.02\,\mathrm{M_\odot\,yr^{-1}}$$

- (see Terreran talk in this session for more on 03gk)

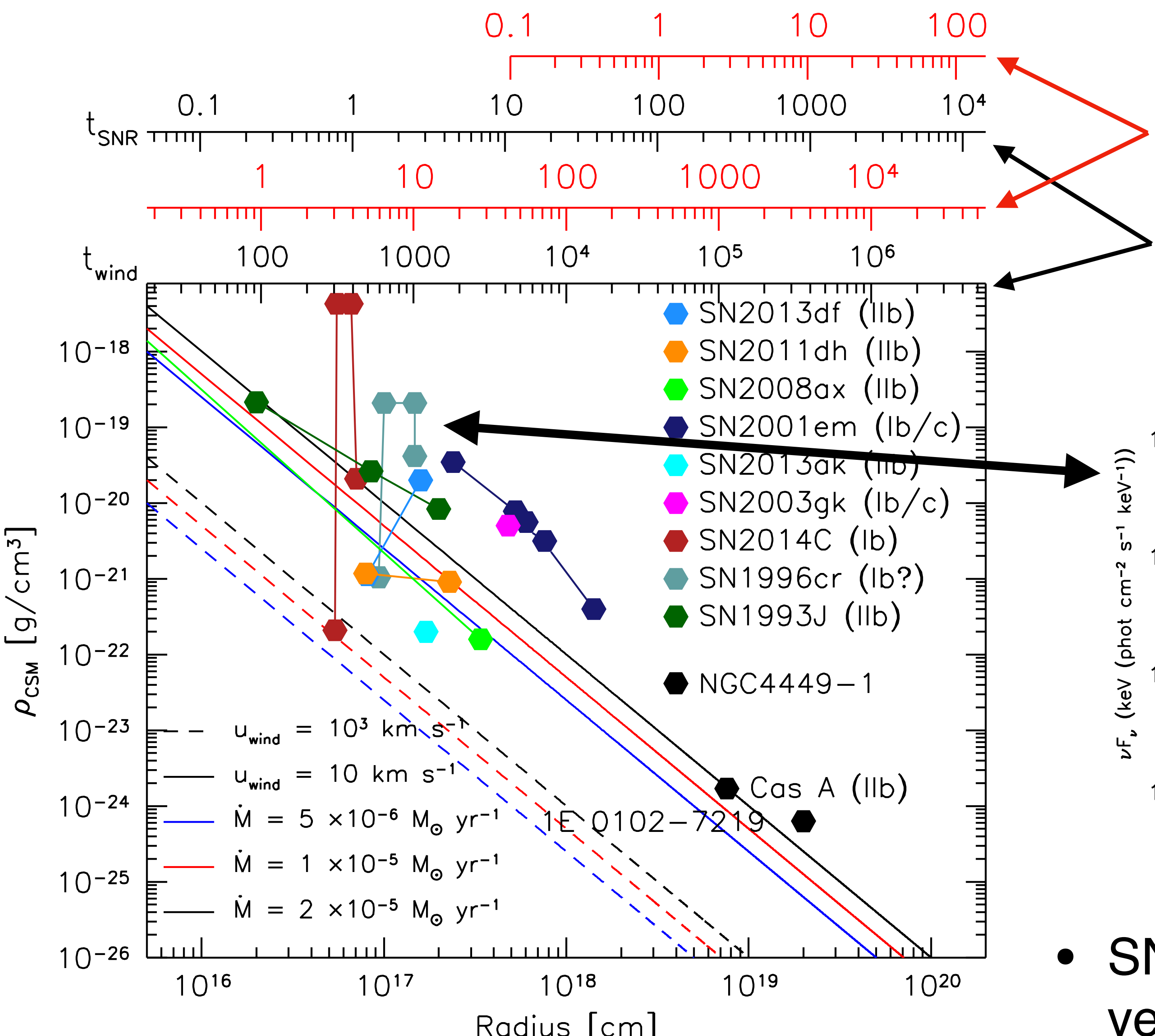

v_{wind} = 10^3 km s^{-1}

v_{wind} = 10 km s^{-1}

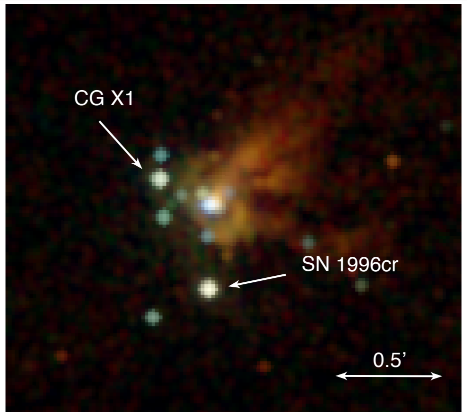

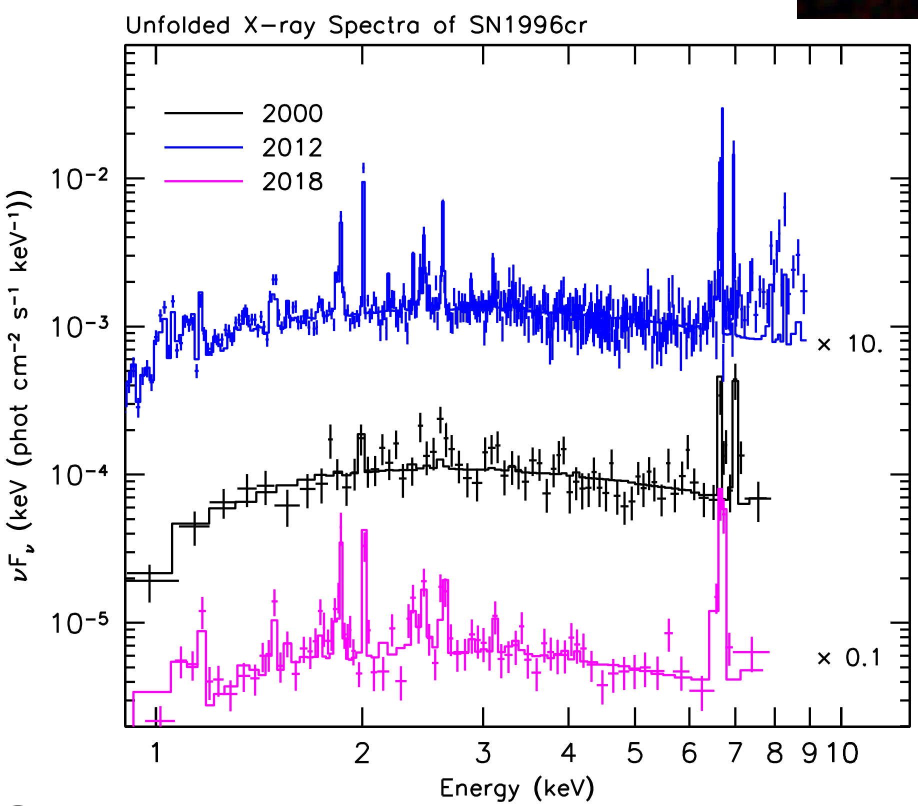

Patnaude et al. (2019; in prep)

CSM properties for several Ib/c and IIb SNe and SNR

- SN1996cr showed extreme brightening ~ 4 years after it is thought to have exploded
- X-ray evolution places cavity at r < 10^{17} cm
- Observations in 2019 suggest that the blastwave has broken out of the shell and is now expanding into the RSG wind

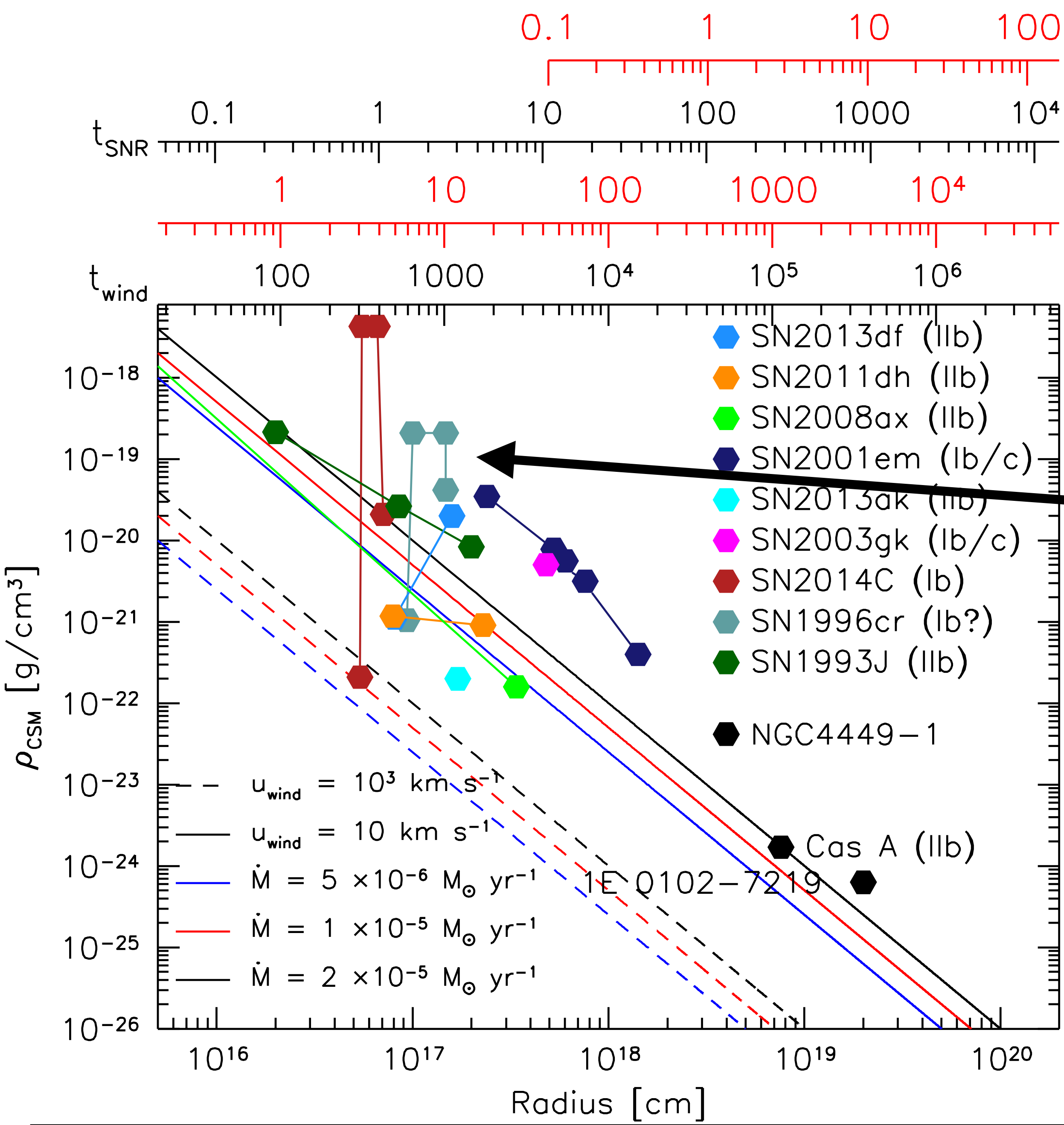

$v_{wind} = 10^3$ km s^{-1}

$v_{wind} = 10$ km s^{-1}

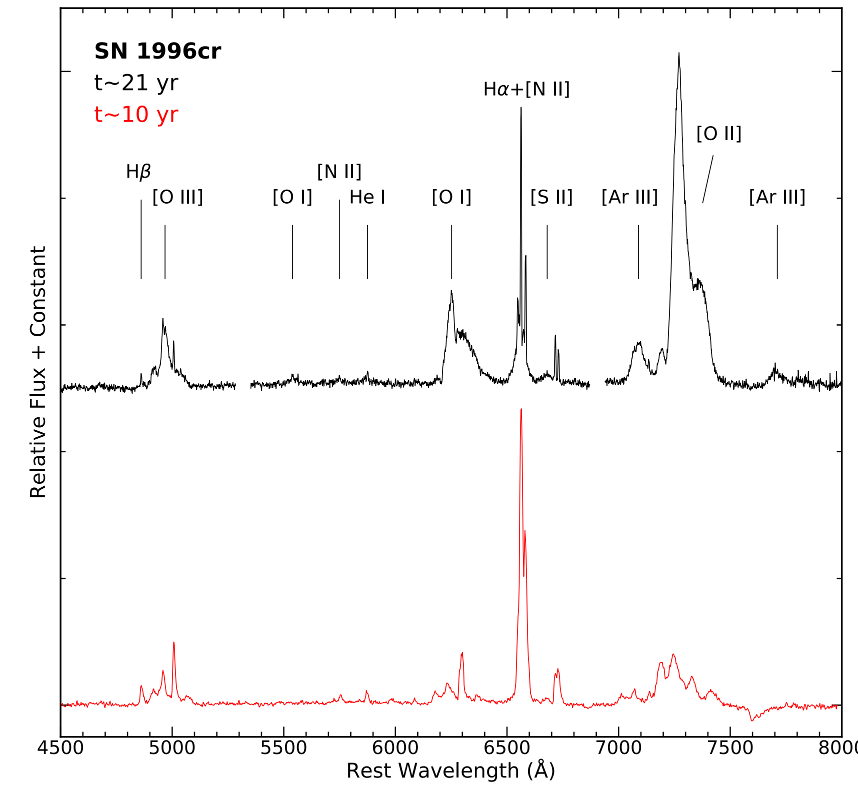

Patnaude et al. (2019; in prep)

CSM properties for several Ib/c and IIb SNe and SNR

- SN1996cr showed extreme brightening ~ 4 years after it is thought to have exploded
- X-ray evolution places cavity at r < 10^{17} cm
- Observations in 2019 suggest that the blastwave has broken out of the shell and is now expanding into the RSG wind

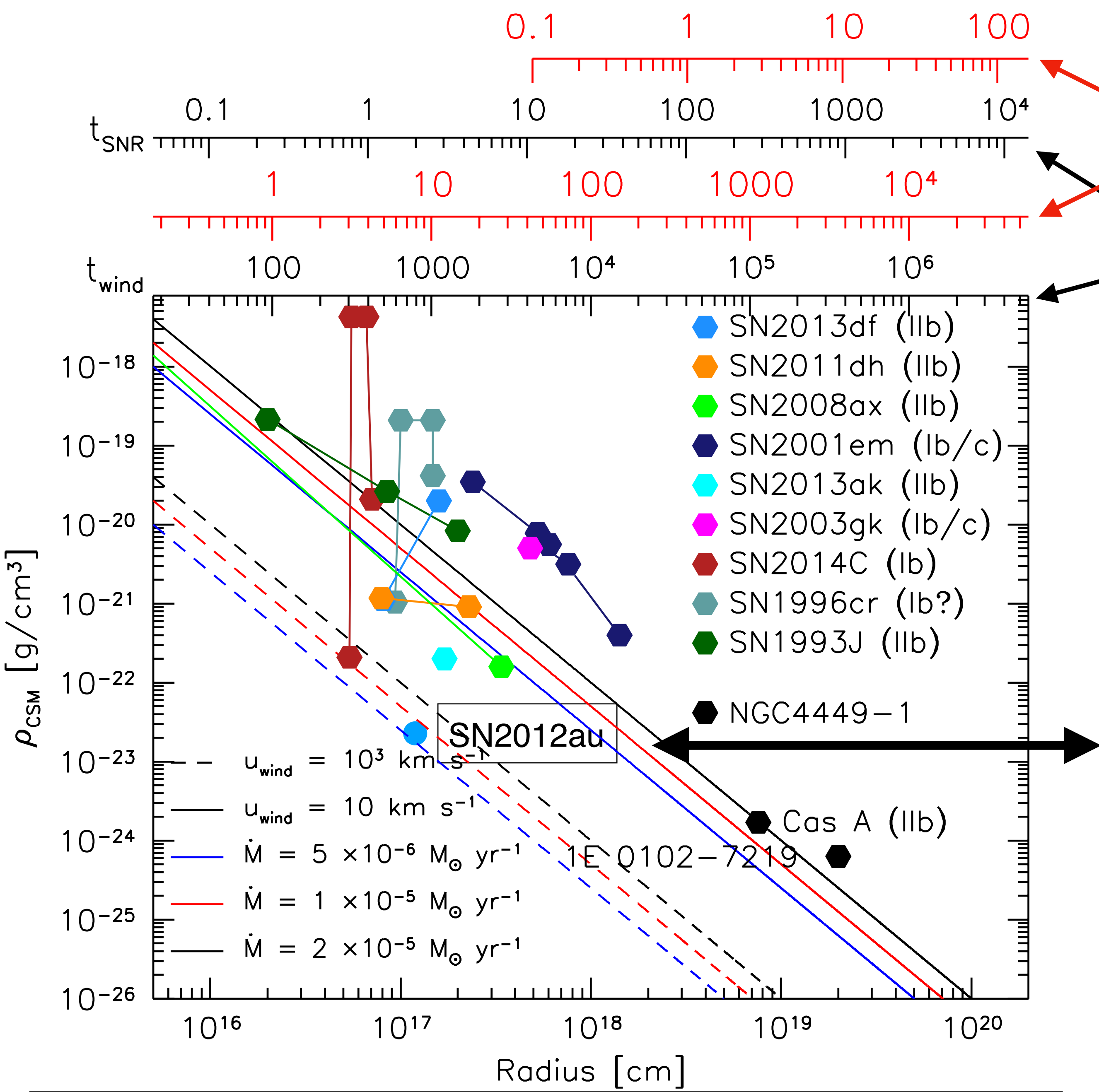

v_{wind} = 10^3 km s^{-1}

v_{wind} = 10 km s^{-1}

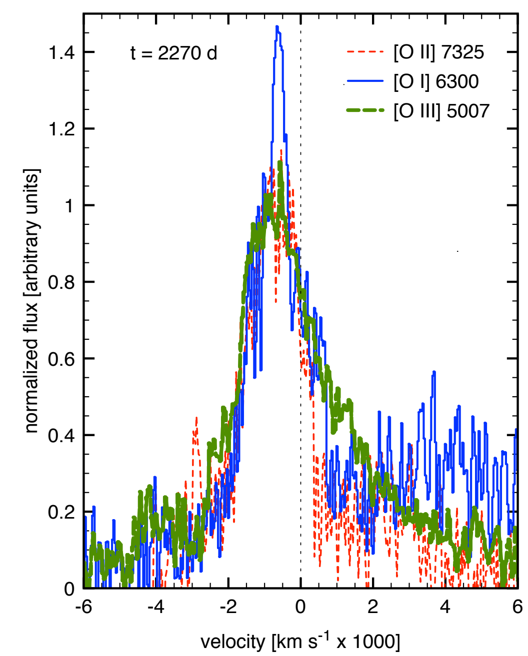

Milisavljevic et al. (2018)

CSM properties for several Ib/c and IIb SNe and SNR

$$L_X < 2 \times 10^{38}\,\mathrm{erg\,s^{-1}}$$

$$\dot{M} \lesssim 4 \times 10^{-6}\,\mathrm{M_\odot\,yr^{-1}}$$

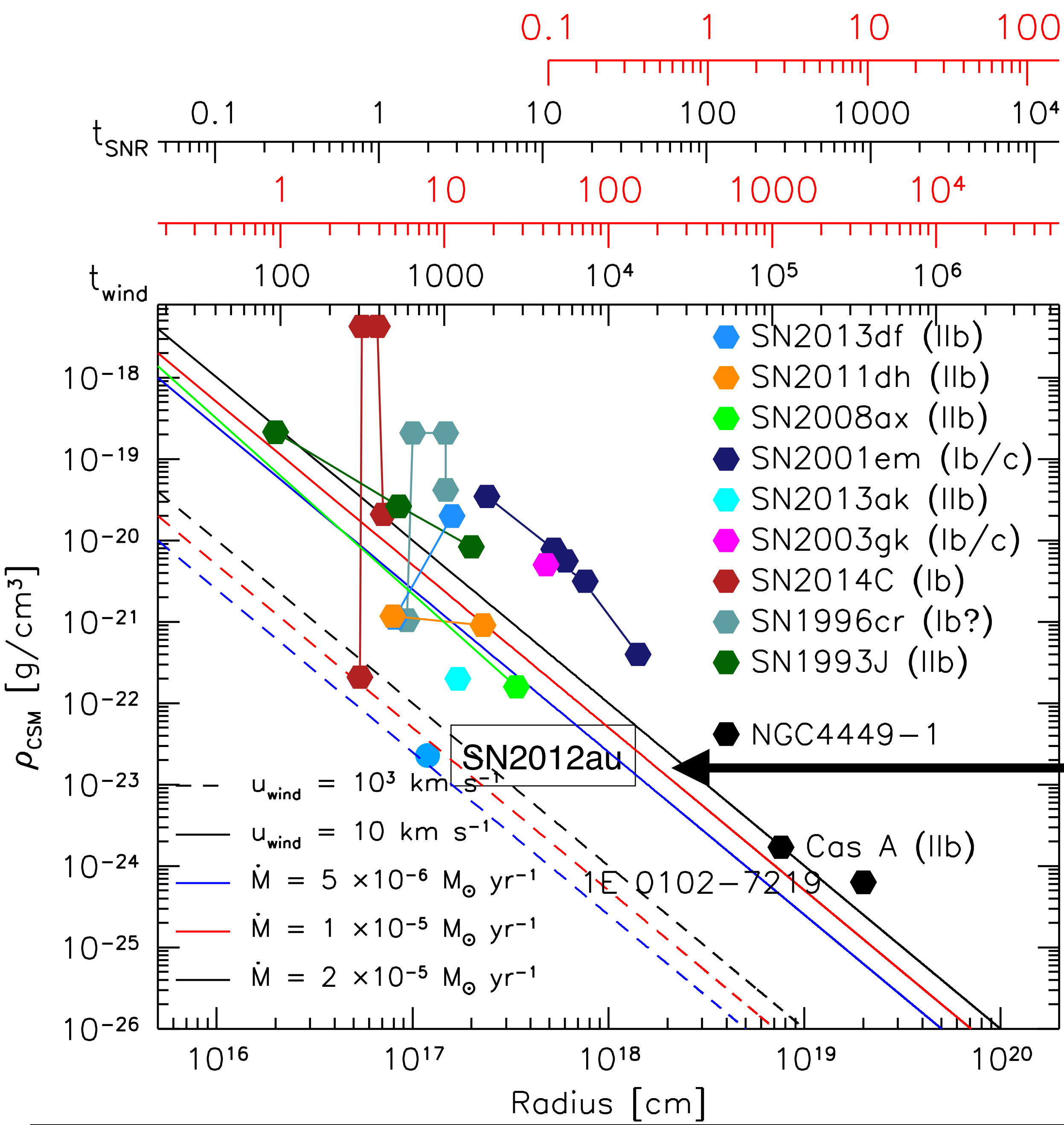

$v_{wind} = 10^3$ km s^{-1}

$v_{wind} = 10$ km s^{-1}

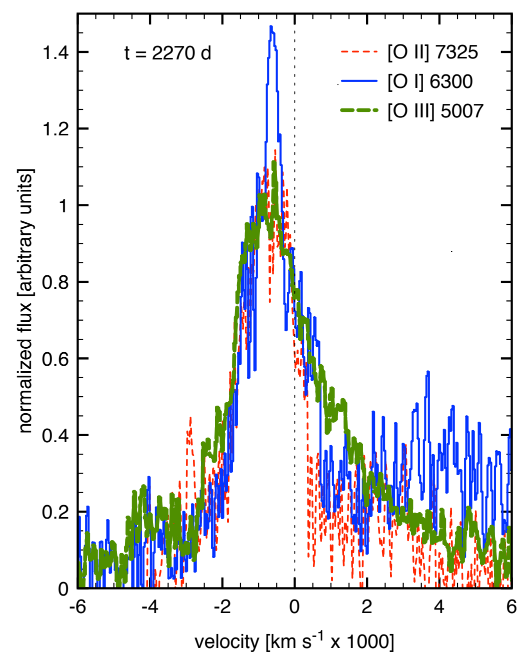

Milisavljevic et al. (2018)

CSM properties for several Ib/c and IIb SNe and SNR

Line velocity widths are consistent with energization from an embedded central engine (see Poster S1.13)

Comparisons to 1D Hydro Models

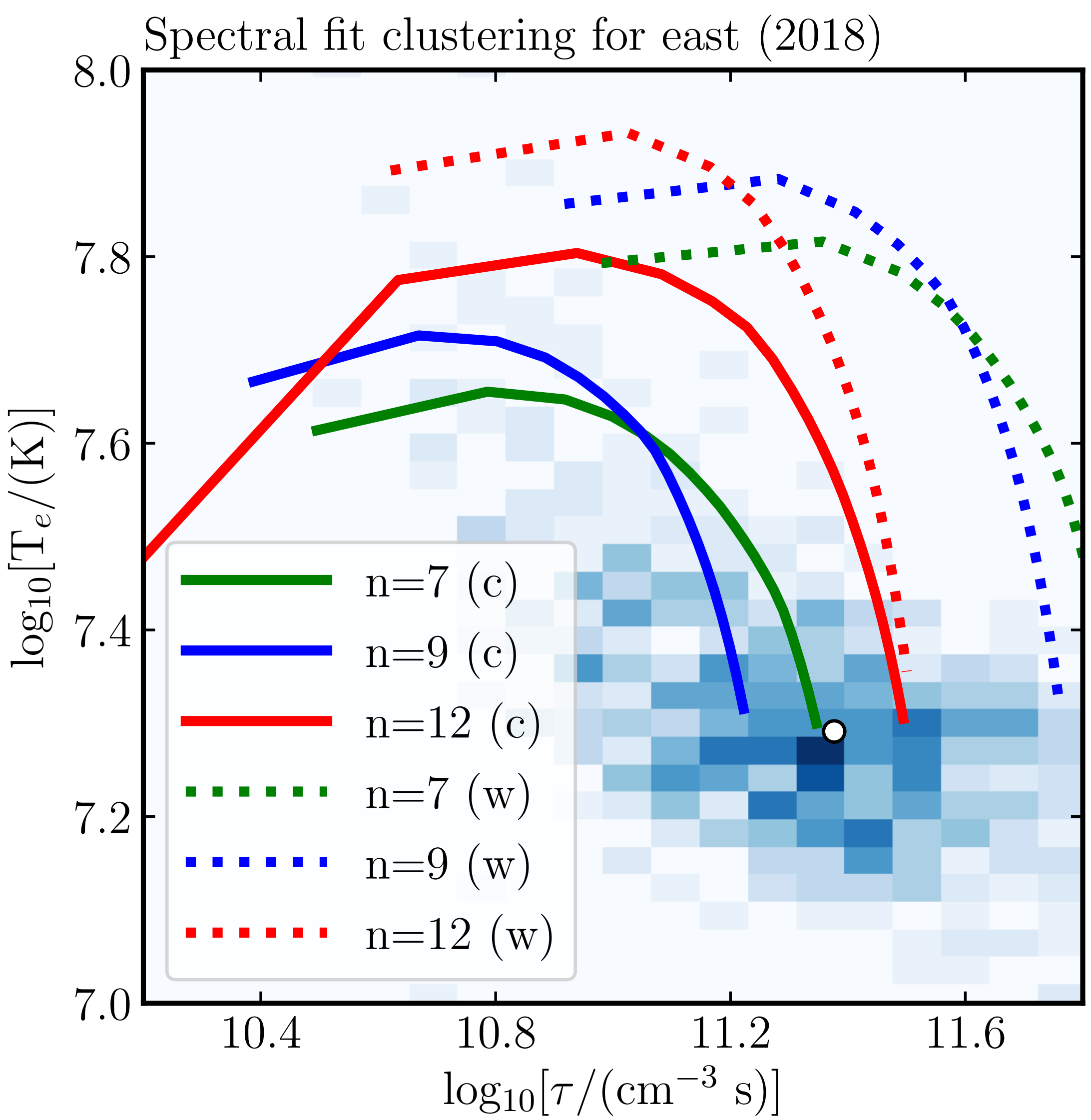

1D models also inform us on large scale azimuthal asymmetries in the ejecta

- In broad terms, different cardinal directions favor different ejecta power law indices

$$E_{\mathrm{SN}} \propto M_{\mathrm{ej}}^{5/7} \frac{(n-3)^{5/3}}{n^{2/3}(n-5)}$$

- When ejecta mass and ejecta core density are held constant, lower values of "n" correspond to higher explosion energies

Comparisons to 1D Hydro Models

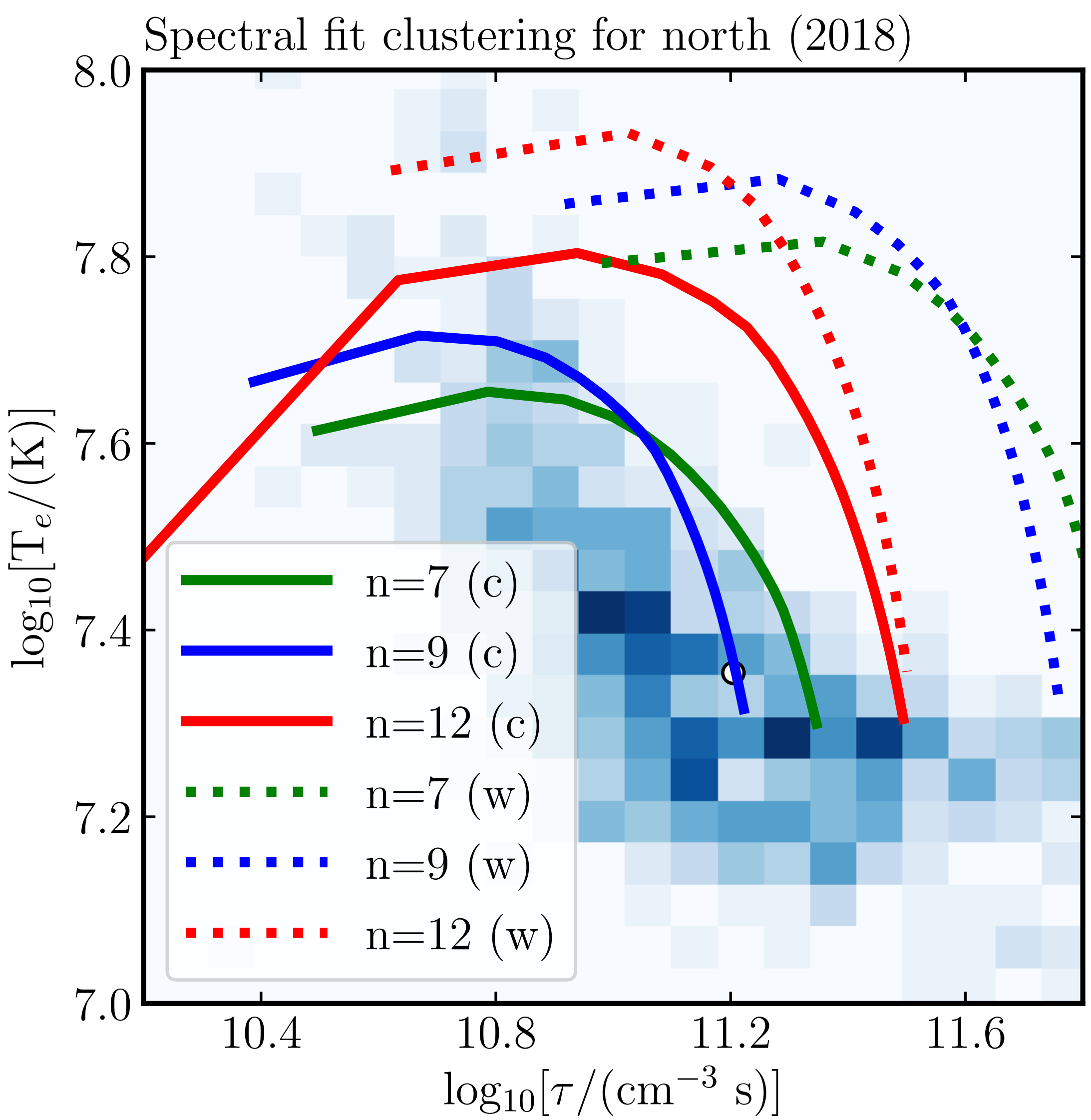

1D models also inform us on large scale azimuthal asymmetries in the ejecta

- In broad terms, different cardinal directions favor different ejecta power law indices

$$E_{\rm SN} \propto M_{\rm ej}^{5/7} \frac{(n-3)^{5/3}}{n^{2/3}(n-5)}$$

- When ejecta mass and ejecta core density are held constant, lower values of "n" correspond to higher explosion energies

Comparisons to 1D Hydro Models

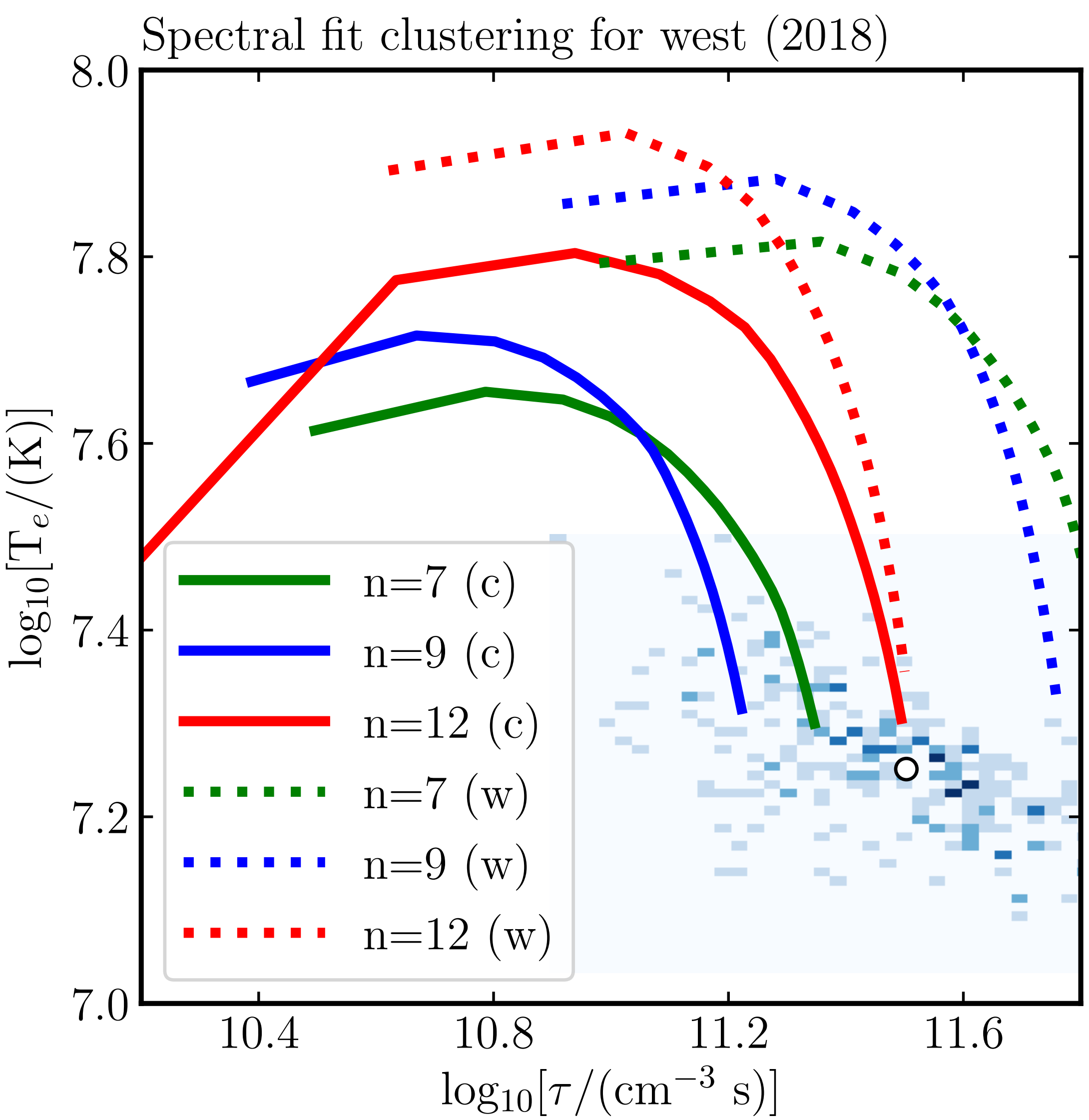

1D models also inform us on large scale azimuthal asymmetries in the ejecta

- In broad terms, different cardinal directions favor different ejecta power law indices

$$E_{\mathrm{SN}} \propto M_{\mathrm{ej}}^{5/7} \frac{(n-3)^{5/3}}{n^{2/3}(n-5)}$$

- When ejecta mass and ejecta core density are held constant, lower values of "n" correspond to higher explosion energies

Conclusions

- X-ray observations of thermal emission from SNR inform us on the properties of both the circumstellar environment and explosion
  - Multi-epoch observations can test 3D models for SNR evolution (e.g., see Orlando talk)
- Multi-epoch X-ray observations of SNe allow us to reconstruct the mass loss history of the progenitor, and light curves reproduce results which are broadly consistent with environments observed around remnants
  - Multiwavelength campaigns allow us to also test models for compact object formation in SNe